PLOS PATHOGENS

RESEARCH ARTICLE

Strain-specific joint invasion and colonization by Lyme disease spirochetes is promoted by outer surface protein C

Yi-Pin Lin[1,2], Xi Tan[3☯], Jennifer A. Caine[4☯], Mildred Castellanos[3], George Chaconas[3], Jenifer Coburn[4]*, John M. Leong[1]*

1 Department of Molecular Biology and Microbiology, Tufts University School of Medicine, Boston, Massachusetts, United States of America, **2** Division of Infectious Diseases, New York State Department of Health, Wadsworth Center, Albany, New York, United States of America, **3** Departments of Biochemistry & Molecular Biology and Microbiology, Immunology & Infectious Diseases, Snyder Institute for Chronic Diseases, University of Calgary, Calgary, Alberta, Canada, **4** Division of Infectious Diseases, and Center for Infectious Disease Research, Medical College of Wisconsin, Milwaukee, Wisconsin, United States of America

☯ These authors contributed equally to this work.
* jcoburn@mcw.edu (JC); John.Leong@tufts.edu (JML)

Citation: Lin Y-P, Tan X, Caine JA, Castellanos M, Chaconas G, Coburn J, et al. (2020) Strain-specific joint invasion and colonization by Lyme disease spirochetes is promoted by outer surface protein C. PLoS Pathog 16(5): e1008516. https://doi.org/10.1371/journal.ppat.1008516

Editor: D. Scott Samuels, University of Montana, UNITED STATES

Received: February 17, 2020

Accepted: April 3, 2020

Published: May 15, 2020

Data Availability Statement: All relevant data are within the manuscript and its Supporting Information files.

Funding: This work was supported by National Institute of Health R01AI37601 (to J.M.L.) and R01AI18799 (to J.C, J.M.L. and G.C.), National Science Foundation IOS1755286 (to Y.L.), Wadsworth Center Start up funds (to Y.L.), and American Heart Association Postdoctoral Fellowship 12POST11660031 (to Y.L.). The sponsors or funders did not play any role in the

Abstract

Lyme disease, caused by *Borrelia burgdorferi*, *B. afzelii* and *B. garinii*, is a chronic, multi-systemic infection and the spectrum of tissues affected can vary with the Lyme disease strain. For example, whereas *B. garinii* infection is associated with neurologic manifestations, *B. burgdorferi* infection is associated with arthritis. The basis for tissue tropism is poorly understood, but has been long hypothesized to involve strain-specific interactions with host components in the target tissue. OspC (outer surface protein C) is a highly variable outer surface protein required for infectivity, and sequence differences in OspC are associated with variation in tissue invasiveness, but whether OspC directly influences tropism is unknown. We found that OspC binds to the extracellular matrix (ECM) components fibronectin and/or dermatan sulfate in an OspC variant-dependent manner. Murine infection by isogenic *B. burgdorferi* strains differing only in their *ospC* coding region revealed that two OspC variants capable of binding dermatan sulfate promoted colonization of all tissues tested, including joints. However, an isogenic strain producing OspC from *B. garinii* strain PBr, which binds fibronectin but not dermatan sulfate, colonized the skin, heart and bladder, but not joints. Moreover, a strain producing an OspC altered to recognize neither fibronectin nor dermatan sulfate displayed dramatically reduced levels of tissue colonization that were indistinguishable from a strain entirely deficient in OspC. Finally, intravital microscopy revealed that this OspC mutant, in contrast to a strain producing wild type OspC, was defective in promoting joint invasion by *B. burgdorferi* in living mice. We conclude that OspC functions as an ECM-binding adhesin that is required for joint invasion, and that variation in OspC sequence contributes to strain-specific differences in tissue tropism displayed among Lyme disease spirochetes.

study design, data collection and analysis, decision to publish, or preparation of the manuscript.

Competing interests: The authors have declared that no competing interests exist.

Author summary

Infection by different Lyme disease bacteria is associated with different manifestations, such as cardiac, neurologic, or, in the case of *B. burgdorferi*, the major cause of Lyme disease in the U.S., joint disease. The basis for these differences is unknown, but likely involve strain-specific interactions with host components in the target tissue. The sequence of the outer surface lipoprotein OspC varies with the strains, and we found that this variation influences the spectrum of host extracellular matrix components recognized. Infection of mice with strains that are identical except for *ospC* revealed that OspC variants that differ in binding spectrum promote infection of different tissues. A strain producing OspC invaded and colonized the joint in living animals, but an altered OspC protein incapable of binding tissue components did not. Thus, tissue-binding by OspC is critical for infection and joint invasion, and OspC variation directly influences tissue tropism.

Introduction

Lyme disease, an infection found throughout the Northern Hemisphere and caused by spirochetes of the genus *Borrelia* (recently renamed *Borreliella* [1]) that are transmitted by *Ixodes* ticks, affects greater than 30,000 people each year in the U.S. alone [2]. An initial skin infection develops at the site of the tick bite, often giving rise to the characteristic 'bull's eye' rash, erythema migrans. Some Lyme disease strains appear to cause only local infections, but many strains spread to other tissues, such as the heart, joints, nervous system or distant skin sites, in the subsequent days or weeks. Weeks to months after initial infection, chronic or late Lyme disease may display distinct clinical syndromes. In the U.S., Lyme borreliosis is caused primarily by *B. burgdorferi* and commonly features arthritis [3]. In contrast, in Europe and Asia, Lyme disease can also be caused by *B. afzelii* and *B. garinii*, which commonly give rise to late stage infections featuring dermatologic or neurologic manifestations, respectively [4–7].

Attachment to host tissues is viewed as an essential early step in colonization [8, 9]. Lyme disease *Borrelia spp*. are highly adhesive and produce at least 19 outer surface proteins that recognize host cells or extracellular matrix (ECM) [9–12]. Remarkably, given the number of these adhesins, mutants that lack one are often detectably diminished both for cell or ECM attachment *in vitro* and for infectivity during experimental animal infection [13–16]. In several instances, adhesin-deficient mutants are selectively defective for colonization of specific tissues. For example, a *B. burgdorferi* mutant deficient for production of the fibronectin-binding adhesin RevA [17] is diminished for colonization of the heart [18, 19], and a mutant deficient in glycosaminoglycan- (GAG-) binding by the surface lipoprotein BBK32 is diminished for colonization of the joint [20].

These findings notwithstanding, the basis for the differences in invasiveness and tissue tropism among Lyme disease spirochetes is poorly understood. Lyme disease spirochetes encode several adhesins that are variable in sequence among different strains, raising the possibility that variable adhesive surface proteins contribute to observed strain- or species-specific differences in tissue tropism and clinical manifestation. In fact, variants of DbpA, an adhesin that binds to the proteoglycan decorin and the glycosaminoglycan (GAG) dermatan sulfate, exhibit differences in GAG- and decorin-binding *in vitro*, and isogenic *B. burgdorferi* strains that differed only in the coding sequence of *dbpA* display differences in tissue tropism upon infection of laboratory mice [21–24].

OspC is a 22 kDa lipoprotein on the surface of *B. burgdorferi* that is not detected when the spirochete is in non-feeding ticks but produced upon the initiation of feeding [25]. OspC plays an essential role in the first days of mammalian infection [26–28]. Furthermore, other than

VlsE, which undergoes extensive antigenic variation during mammalian infection, OspC displays the highest inter-strain variability of any Lyme disease spirochete proteins [29–31]. The central portion of OspC is highly variable [32, 33] and OspC variants fall into one of 22 classes, termed A through U, with at least 8% variability separating different groups [34–36]. Notably, a subset of OspC classes are produced by *Borrelia* strains and species associated with disseminated infections in humans and/or mice [7, 34, 35, 37–40]. OspC binds to the host protease precursor, plasminogen, *in vitro* [37, 41] and inhibits the phagocytosis of spirochetes by macrophages *ex vivo* [42], although direct evidence linking these activities of OspC to infectivity in the mammalian host remains to be developed. Recently, OspC of *B. burgdorferi* strain B31 was shown to promote bloodstream survival in mice and inhibit activation of the classical and lectin complement pathways *in vitro* [43]. The formation of the C4b2a complex by factors C4 and C2 is critical for the activation of these pathways, and this OspC variant and C2 were shown to bind to human C4b in a mutually exclusive manner. However, an OspC variant that does not bind human C4b still promotes bloodstream survival in mice [43], indicating that the role that OspC plays during mammalian infection remains incompletely understood.

OspC is orthologous to Vsps (variable small proteins), which are antigenically variable surface proteins encoded by relapsing fever borreliae, such as *Borrelia turicatae* and *B. hermsii* [44, 45], and shares overlapping function with a member of this family, Vtp, that is expressed upon acquisition of the blood meal [46]. *B. turicatae* variant Vsp2 but not Vsp1 recognizes GAGs [47], and *B. turicatae* production of Vsp2 rather than Vsp1 is associated with seven- to eight-fold better colonization of the blood and joint [48]. These data suggest that Vsps, and by inference, perhaps OspC, influence tissue tropism of pathogenic *Borrelia* by binding ECM components such as GAGs. Finally, when a library of phages displaying *B. burgdorferi* protein fragments on the surface was inoculated intravenously (*i.v.*) into mice, phages producing OspC peptides were enriched in the heart and joints [49], reinforcing the possibility that OspC may function as an adhesin. However, evidence that OspC promotes spirochetal interaction with host cells or ECM is lacking. Furthermore, colonization of target tissue is a multistep process [8, 9, 50], and the pathogenic consequence of a putative interaction between surface-localized OspC and host tissue is completely unexplored.

In the current study, we found that OspC confers variant-specific binding of the bacteria to dermatan sulfate and/or fibronectin. Murine infection by isogenic *B. burgdorferi* strains that differ only in *ospC* coding sequence revealed that OspC variation results in differences in joint colonization. An OspC mutant incapable of binding either dermatan sulfate or fibronectin was dramatically deficient in tissue colonization and found in tissues at levels no higher than an OspC-defective strain. Intravital microscopy revealed that this OspC mutant, in contrast to wild type OspC, was defective in promoting vascular transmigration into knee joint tissues by *B. burgdorferi* in living animals. We conclude that OspC functions as an adhesin that promotes joint invasion, and that the variation in OspC sequence contributes to strain-specific differences in tissue tropism displayed by Lyme disease spirochetes.

Results

Recombinant OspC protein of *B. burgdorferi* sensu stricto N40-D10/E9 binds to fibronectin and dermatan sulfate

Previous work has revealed that many Lyme borreliae surface proteins bind ECM components [17, 50–57], and OspC was previously identified as a candidate adhesin [49], so we generated a GST fusion protein of OspC that encompasses the mature sequence but lacks the (cleaved) signal peptide of *B. burgdorferi* strain N40-D10/E9 ("$OspC_{N40\text{-}D10/E9}$") and assessed its ability to bind a number of ECM components, including fibronectin, laminin, collagen, and a variety of

GAGs immobilized in microtiter wells. ELISA detection of bound GST-$OspC_{N40\text{-}D10/E9}$ using anti-GST antibody revealed that fibronectin and dermatan sulfate GAG were recognized by GST-$OspC_{N40\text{-}D10/E9}$ but not GST (Fig 1). No other substrates tested were recognized by this protein.

To estimate the dissociation constants for binding of dermatan sulfate or fibronectin to GST-$OspC_{N40\text{-}D10/E9}$, varying concentrations of GST-$OspC_{N40\text{-}D10/E9}$ or, as a control, GST alone, were incubated in wells coated with purified dermatan sulfate or fibronectin, and binding was determined by ELISA (Fig 2, left panels). $OspC_{N40\text{-}D10/E9}$ bound to dermatan sulfate with an estimated K_D of 0.16μM and to fibronectin with an estimated K_D of 0.35μM (Fig 2, left panels, and Table 1). To independently assess the dissociation constants of $OspC_{N40\text{-}D10/E9}$, binding to dermatan sulfate or fibronectin was tested by surface plasmon resonance (SPR; Fig 2, right panels). These experiments revealed k_{on} and k_{off} rates that result in calculated K_D's of binding of $OspC_{N40\text{-}D10/E9}$ to dermatan sulfate or fibronectin to be 0.25μM or 0.30μM, respectively, i.e. consistent with the K_D's determined by ELISA (Table 1).

Recombinant OspC variants exhibit distinct fibronectin- and dermatan sulfate-binding activities

OspC demonstrates sequence variability among different strains [32]. To determine if OspC variants among strains of Lyme disease spirochetes differ in their adhesive activity to dermatan sulfate and fibronectin, GST-OspC proteins from OspC of *B. burgdorferi* strains B31-A3 ($OspC_{B31}$) and 297 ($OspC_{297}$), *B. garinii* strain PBr ($OspC_{PBr}$), and *B. afzelii* strain VS461

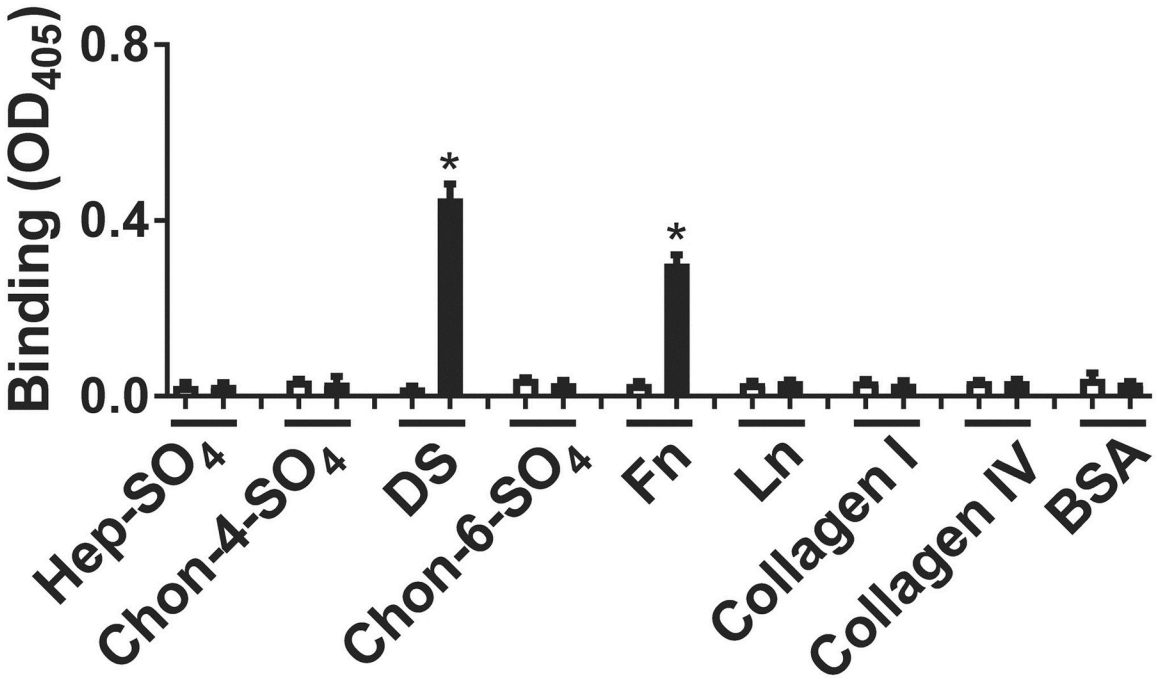

Fig 1. Recombinant $OspC_{N40\text{-}D10/E9}$ binds to fibronectin and dermatan sulfate. Quadruplicate wells were incubated with 10 μg/ml of heparan sulfate (Hep-SO_4), chondroitin-4-sulfate (Chon-4-SO_4), dermatan sulfate (DS), chondroitin-6-sulfate (Chon-6-SO_4), fibronectin (Fn), laminin (Ln), type I collagen (Collagen I), type IV collagen (Collagen IV) or BSA (see Materials and Methods). Two μM recombinant GST-tagged $OspC_{N40\text{-}D10/E9}$ (black bars) or GST (negative control; white bars) was then added to the wells. Bound protein was measured by ELISA and mean OD_{405} ± SEM was determined. Asterisks indicate that binding of GST-OspC to dermatan sulfate or fibronectin was significantly ($p \leq 0.05$) greater than binding by GST by Student's t-test. Shown is a representative of three independently performed experiments.

https://doi.org/10.1371/journal.ppat.1008516.g001

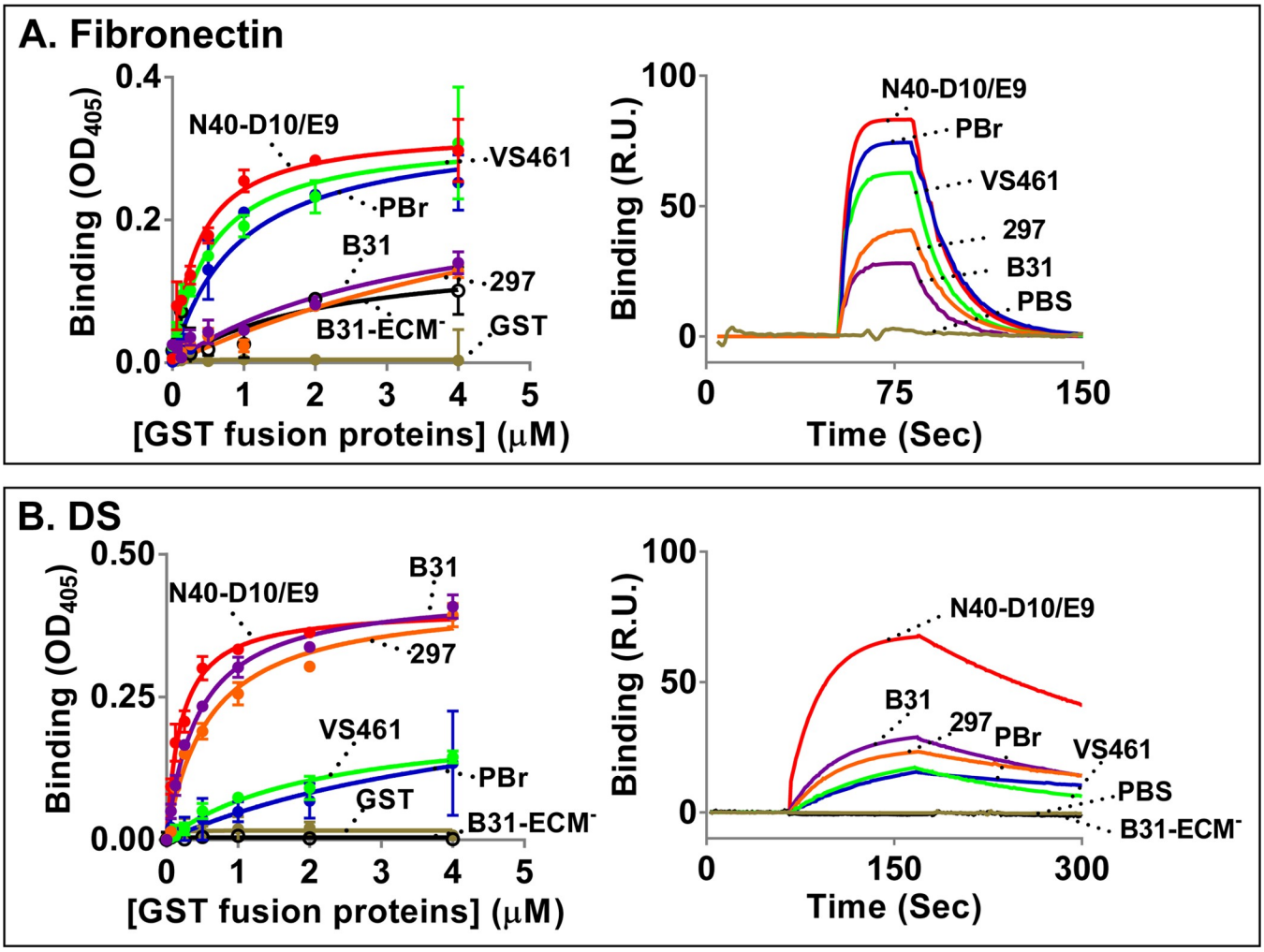

Fig 2. Recombinant OspC variants exhibit distinct fibronectin- and dermatan sulfate-binding activities. (A) Left panel: Quadruplicate wells were incubated with 10 μg/ml of fibronectin. The indicated concentrations of various recombinant GST-tagged OspC variants, including $OspC_{B31}$ ("B31"), $OspC_{N40\text{-}D10/E9}$ ("N40-D10/E9"), $OspC_{297}$ ("297"), $OspC_{PBr}$ ("PBr"), $OspC_{VS461}$ ("VS461"), $OspC_{B31\text{-}ECM^-}$ ("B31-ECM$^-$"), or GST (as a negative control), were then added to the wells. The protein binding was quantified by ELISA. The K_D values were obtained from the average of three independent experiments and shown on Table 1. Shown is a representative of three experiments with numbers indicating the mean ± standard deviation derived from quadruplicate wells. **Right panel:** Ten μg of fibronectin in 10 μl was allowed to flow through CM5 chips. 15.625 to 500 nM of the indicated untagged OspC protein was then flowed over the chips. Binding was measured in response units (R.U.) by SPR. Shown is the binding of 500nM of indicated OspC proteins to fibronectin from one experiment as a representative of six experiments performed on three different occasions. The K_D values were obtained from average of the six experiments and shown in Table 1. **(B) Left panel:** Quadruplicate wells were incubated with 10 μg/ml of dermatan sulfate (DS). Indicated GST-tagged OspC variants were then added to the wells, as described in Panel A. The K_D values were obtained from the average of three independent experiments and shown in Table 1. Shown is a representative of the three experiments with numbers indicating the mean ± standard deviation derived from quadruplicate wells. **Right panel:** Ten μg of biotinylated dermatan sulfate in 10 μl was allowed to flow through SA chips.15.625 to 500 nM of the indicated untagged OspC variants was then flowed over the chips, as described in panel A. Shown is the binding of indicated OspC proteins to dermatan sulfate from one experiment as a representative of six experiments performed on three different occasions. The K_D values were obtained from average of the six experiments and shown in Table 1.

https://doi.org/10.1371/journal.ppat.1008516.g002

($OspC_{VS461}$), all of which belong to different OspC classes [7, 36] were tested for binding to dermatan sulfate and fibronectin by ELISA whereas these OspC variants without GST tags were examined for the binding to these ECM ligands by SPR (Fig 2). Estimated dissociation constants were calculated for each interaction using both ELISA and SPR, and the two methods gave highly consistent results (Table 1). Interestingly, the OspC variants demonstrated considerable differences in their recognition of fibronectin and dermatan sulfate: $OspC_{VS461}$ and $OspC_{PBr}$ bound preferentially to fibronectin (K_D~0.5–0.9 μM) as compared to dermatan

Table 1. OspC variants differ in binding to dermatan sulfate and fibronectin.

		ELISA	——— Surface Plasmon Resonance ———		
OspC variant	**Ligand**	**K_D (μM)**	**K_D (μM)**	**k_{on} ($10^4 s^{-1}M^{-1}$)**	**k_{off} (s^{-1})**
B. burgdorferi					
$OspC_{N40\text{-}D10/E9}$	**Derm $S0_4$**	**0.16±0.05**	**0.27±0.07**[a]	4.64±1.94[a]	0.01±0.003[a]
	Fibronectin	**0.35±0.03**	**0.30±0.07**[a]	45.08±14.94[a]	0.13±0.04[a]
$OspC_{B31}$	**Derm $S0_4$**	**0.40±0.07**	**0.57±0.17**[a]	1.71±0.17[a]	0.01±0.004[a]
	Fibronectin	**3.46±1.46**[b]	**9.21±4.04**[a,b]	1.99±0.70[a]	0.13±0.05[a]
$OspC_{B31\text{-}ECM\text{-}}$	**Derm $S0_4$**	**n.b.**[c]	**n.b.**[c]	n.b.[c]	n.b.[c]
	Fibronectin	**2.14±1.82**[b]	**n.d.**[d]	n.d.[d]	n.d.[d]
$OspC_{297}$	**Derm $S0_4$**	**0.60±0.13**	**0.75±0.32**[a]	1.69±0.35[a]	0.01±0.002[a]
	Fibronectin	**2.78±1.46**[b]	**1.75±0.40**[a,b]	3.68±0.24[a]	0.06±0.005[a]
B. garinii					
$OspC_{PBr}$	**Derm $S0_4$**	**5.53±3.92**[b]	**9.97±2.19**[a,b]	0.040±0.001[a]	0.003±0.001[a]
	Fibronectin	**0.90±0.20**	**0.71±0.08**[a]	19.20±5.95[a]	0.13±0.04[a]
B. afzelii					
$OspC_{VS461}$	**Derm $S0_4$**	**2.01±0.31**[b]	**4.21±1.10**[a,b]	0.042±0.002[a]	0.002±0.001[a]
	Fibronectin	**0.52±0.08**	**0.80±0.34**[a]	15.06±3.94[a]	0.09±0.03[a]

All values represent the mean ± SEM of three experiments.

[a]The K_D values were obtained from the average k_{off} divided k_{on} from each run.

[b]The values should be considered estimates due to the weakness of the interaction.

[c]No binding activity was detected.

[d]Not determined.

https://doi.org/10.1371/journal.ppat.1008516.t001

sulfate (K_D ~2.0–10.0 μM), whereas $OspC_{B31}$ and $OspC_{297}$ bound preferentially to dermatan sulfate (K_D ~0.4–0.8 μM) as compared to fibronectin (K_D ~1.7–9.2 μM) (Fig 2 and Table 1).

B. burgdorferi OspC promotes adhesion to the joint vasculature in a one-hour intravenous inoculation model

Because OspC was selected for binding to the vasculature of living mice shortly after *i.v.* inoculation of a phage display library [49], we tested the role of the protein as produced by *B. burgdorferi* in mediating very early interactions with the vasculature of the ankle joint in our 1 hr *i.v.* inoculation model [18]. We produced OspC variants in an *ospC*-deficient mutant of *B. burgdorferi* strain B31-A3 [28], utilizing pBSV2G-derived *ospC*-complementing plasmids that are identical except for their *ospC* coding sequences (i.e. $ospC_{B31}$, $ospC_{N40\text{-}D10/E9}$, or $ospC_{PBr}$). For this short-term infection model, all *ospC* genes were cloned 3' to the *flaB* promoter to ensure protein production by *in vitro* cultivated bacteria. One hour after inoculation, all of the strains were able to localize to the joint at detectable levels, consistent with the expression of lipoproteins such as BBK32 and DbpA, which promote joint adhesion [9, 20, 22, 50]. Nevertheless, $OspC_{B31}$ and $OspC_{N40\text{-}D10/E9}$ promoted *B. burgdorferi* adhesion to the vasculature of the ankles in living mice at levels similar to the parental B31-A3, while the numbers of bacteria producing no OspC (*ΔospC*) or $OspC_{PBr}$ were significantly reduced in comparison (Fig 3).

Generation of an OspC mutant that is defective for binding to dermatan sulfate and fibronectin

To better study the contribution of ECM binding by OspC, targeted mutations were made to generate recombinant OspC protein lacking both fibronectin- and dermatan sulfate-binding

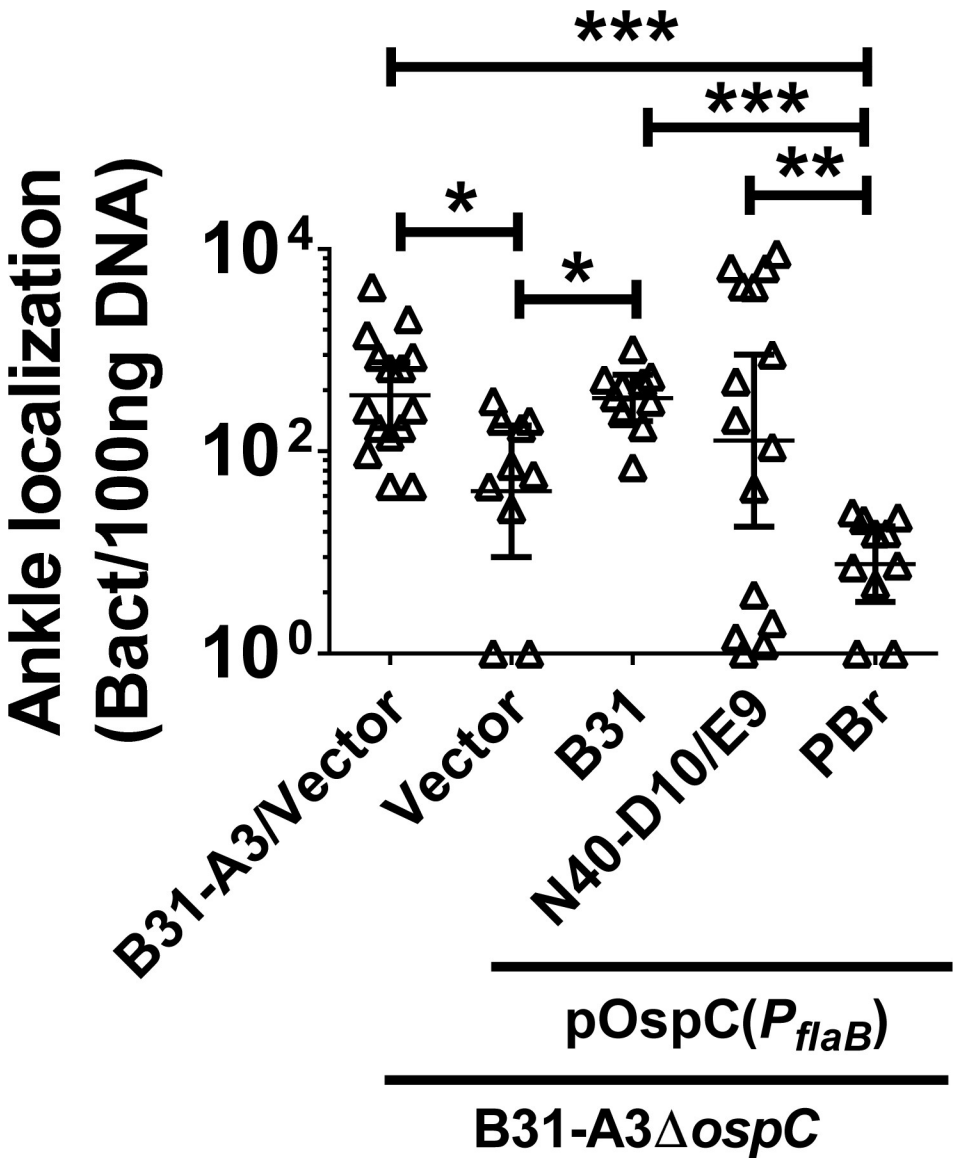

Fig 3. OspC promotes ankle joint localization of spirochetes in an allele-specific manner one hour after intravenous inoculation. C3H/HeN mice were inoculated retro-orbitally with infectious *B. burgdorferi* strain B31-A3 with the vector pBSV2G ("B31-A3/Vector"), B31-A3Δ*ospC* with the vector ("Vector"), or B31-A3Δ*ospC* producing OspC from B31-A3 ("B31"), *B. burgdorferi* strain N40 clone D10/E9 ("N40-D10/E9"), or *B. garinii* strain PBr ("PBr"). After 1 hr, perfused tissues were collected and bacterial burdens were quantified by qPCR. Data are shown as the geometric mean ± 95% confidence interval. Statistical significance was determined using ANOVA with the Kruskal-Wallis test followed by the two-stage step-up method of Benjamini, Krieger and Yekutieli. * = $P < 0.05$, ** = $P < 0.01$, *** = $P < 0.001$. N = 10 or 15 mice per *B. burgdorferi* strain.

https://doi.org/10.1371/journal.ppat.1008516.g003

activity. We focused on a 61-residue segment in the central region of OspC that was previously found to be common to all surface display phage enriched for tissue targeting after *i.v.* infection of mice (S1 Fig) [49]. Basic residues have been shown to be critical for activity by other GAG-binding proteins [58], and of five residues 116, 121, 123, 128, and 129, located in α-helix 3 and loop 4, all are lysines in the dermatan sulfate-binding variants $OspC_{B31}$ and $OspC_{297}$, and four of the five are lysines in $OspC_{N40\text{-}D10/E9}$, which also binds dermatan sulfate (S2A and s2B Fig). In contrast, only three and two of these residues are lysines in the variants $OspC_{VS461}$

and $OspC_{PBr}$, respectively, which do not efficiently bind to dermatan sulfate. Wild type $OspC_{B31}$ binds inefficiently to fibronectin (K_D ~3.5 μM, Table 1), so to generate an OspC derivative lacking both high-level fibronectin- and dermatan sulfate-binding activity, the five $OspC_{B31}$ lysine residues in this region of $OspC_{B31}$ were mutated to methionine. Maintenance of secondary structure of this derivative, which we termed "$OspC_{B31\text{-}ECM^-}$", was confirmed by circular dichroism (CD) analysis (S2C Fig). In addition, $OspC_{B31\text{-}ECM^-}$ and wild type $OspC_{B31}$ bound to C4b indistinguishably, indicating that the structure of the protein is not dramatically altered by the substitutions and that the lysine residues are not required for C4b-binding activity (S2D Fig). ELISA analysis demonstrated that the fibronectin-binding activity of the mutant protein remained poor (K_D ~2.1 μM), and its dermatan sulfate-binding activity was undetectable (Fig 2 and Table 1).

B. burgdorferi producing OspC variants differ in their ability to bind to fibronectin and dermatan sulfate

We investigated whether the different degrees of dermatan sulfate- or fibronectin-binding by OspC variants in purified recombinant form correspond to their ability to mediate spirochetal binding to these substrates when expressed on the surface of the bacterium. To interrogate a set of OspC variants that together encompass a wide variety of binding phenotypes, we analyzed: (a) $OspC_{B31\text{-}ECM^-}$, which recognizes neither fibronectin or dermatan sulfate efficiently; (b) $OspC_{B31}$, which efficiently recognizes dermatan sulfate but not fibronectin; (c) $OspC_{N40\text{-}D10/E9}$, which efficiently binds both fibronectin and dermatan sulfate; and (d) $OspC_{PBr}$, which recognizes fibronectin but not dermatan sulfate (Table 1). We produced these OspC variants in the *ospC*-deficient mutant of *B. burgdorferi* strain B31-A3 [28], utilizing pBSV2G-derived *ospC*-complementing plasmids that are expressed by the $ospC_{B31}$ promoter in order to mimic the expression level of endogenous *ospC*, but differ in their *ospC* coding sequences. (These plasmids encoding $ospC_{B31}$, $ospC_{B31\text{-}ECM^-}$, $ospC_{N40\text{-}D10/E9}$, and $ospC_{PBr}$ were termed $pOspC_{B31}$, $pOspC_{B31\text{-}ECM^-}$, $pOspC_{N40\text{-}D10/E9}$, and $pOspC_{PBr}$, respectively). Flow cytometric quantitation of the surface production levels of all OspC variants or mutants (see Materials and Methods) indicated that all were efficiently displayed on the spirochetal surface, indistinguishably from the level of OspC on the surface of *B. burgdorferi* strain B31-A3 carrying pBSV2G (vector) alone (S3 Fig).

These strains, as well as *B. burgdorferi* strain B31-A3Δ*ospC*/pBSV2G, were radiolabeled and incubated in wells coated with purified fibronectin. After washing, stably bound bacteria were quantitated by scintillation counting. BSA-coated wells, used as a negative control, were found to consistently immobilize less than 5% of the inoculum (Fig 4, top panel). *B. burgdorferi* strain B31-A3/pBSV2G bound to fibronectin significantly better than to control wells (Fig 4, "B31-A3/Vector", middle panel), consistent with the presence of outer surface proteins, such as BBK32, RevA, and BB0347, that promote binding to this ECM protein [17, 50–52]. As expected, given that GST-$OspC_{B31}$ does not recognized fibronectin, strain B31-A3Δ*ospC*/pBSV2G (Fig 4, "Vector", middle panel) demonstrated no defect in fibronectin binding compared to wild type strain B31-A3, and ectopic production of $OspC_{B31}$ by this strain did not enhance fibronectin binding (Fig 4, "B31", middle panel). Similarly, ectopic production of $OspC_{B31\text{-}ECM^-}$ by strain B31-A3Δ*ospC* did not enhance fibronectin binding (Fig 4, "B31-ECM$^-$", middle panel). In contrast, B31-A3Δ*ospC* harboring plasmids producing $OspC_{N40\text{-}D10/E9}$ or $OspC_{PBr}$, both of which as GST-fusion proteins efficiently recognize fibronectin, resulted in enhanced fibronectin-binding by B31-A3Δ*ospC* (Fig 4, "N40-D10/E9" and "PBr", middle panel). Hence, the fibronectin-binding properties of the OspC variants determined using recombinant protein are reflected in their ability to promote fibronectin-binding by *B. burgdorferi*.

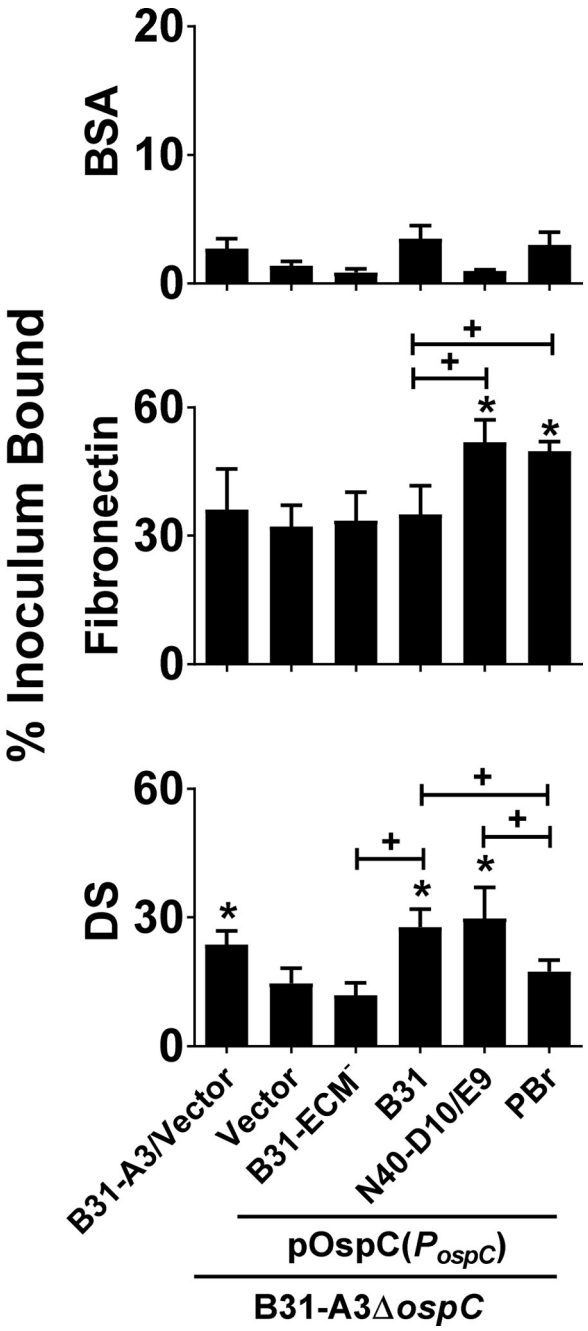

Fig 4. *B. burgdorferi* producing OspC variants differ in their ability to bind to fibronectin and dermatan sulfate. Binding of radiolabeled *B. burgdorferi* B31-A3/pBSV2G ("B31-A3/Vector"), *ospC*-deficient strain B31-A3Δ*ospC*/pBSV2G ("Vector"), or the deletion strain bearing a plasmid encoding the indicated OspC variants to BSA **(Top panel)**, fibronectin **(Middle panel),** or dermatan sulfate (DS) **(Bottom panel)** was determined (see Materials and Methods). Each bar represents the mean of four independent determinations ± SEM. Statistical significance was determined using ANOVA with the Kruskal-Wallis test followed by the two-stage step-up method of Benjamini, Krieger and Yekutieli. Significant ($p < 0.05$) differences in binding relative to the OspC-deficient strain B31-A3Δ*ospC*/pBSV2G ("*") or between two strains relative to each other ("+") are indicated.

https://doi.org/10.1371/journal.ppat.1008516.g004

These strains were also tested for binding to immobilized dermatan sulfate. *B. burgdorferi* strain B31-A3/pBSV2G (Fig 4, "B31-A3/Vector", bottom panel) bound to dermatan sulfate

significantly better (23% vs. 14%) than did B31-A3Δ*ospC* harboring control vector (Fig 4, "Vector", bottom panel), indicating that OspC produced by this strain promotes spirochetal binding to dermatan sulfate. Notably, the lower level of dermatan sulfate-binding by the *ospC*-deficient derivative of B31-A3 was still higher than binding to control wells, consistent with the presumed expression of other dermatan sulfate-binding proteins such as BBK32, Bgp, DbpB and DbpA [54, 55, 59–61]. Ectopic expression of $OspC_{B31}$ from $pOspC_{B31}$ complemented the relative defect in dermatan sulfate binding by the *ospC*-deficient strain (Fig 4, "B31", bottom panel), and complementation of binding required dermatan sulfate-binding activity because ectopic production of $OspC_{B31\text{-}ECM^-}$, which does not exhibit dermatan sulfate-binding activity as a GST fusion protein, did not result in enhanced binding (Fig 4, "B31-ECM$^-$", bottom panel). Similarly, ectopic expression of $OspC_{PBr}$, which also lacks dermatan-sulfate binding as a recombinant protein, did not increase binding by B31-A3Δ*ospC* (Fig 4, "PBr", bottom panel). Finally, as predicted given the ability of GST-$OspC_{N40\text{-}D10/E9}$ to bind dermatan sulfate, production of $OspC_{N40\text{-}D10/E9}$ by B31-A3Δ*ospC* significantly enhanced GAG binding. Thus, the fibronectin- and dermatan sulfate-binding activities of each OspC variant that were determined by ELISA and SPR (Table 1) correlated with their ability to promote spirochetal binding to the two substrates.

OspC of *B. burgdorferi* sensu stricto strains B31-A3 and N40-D10/E9, but not *B. garinii* strain PBr, promote joint colonization and swelling

To determine if sequence variation of *ospC* results in difference of tissue colonization, C3H/HeN mice were intradermally inoculated with $1x10^4$ *B. burgdorferi* strain B31-A3/pBSV2G (Fig 5A, "B31-A3/Vector"), B31-A3Δ*ospC*/pBSV2G ("Vector"), or B31-A3Δ*ospC* producing $OspC_{B31\text{-}ECM^-}$ ("B31-ECM$^-$")., $OspC_{B31}$ ("B31"), $OspC_{N40\text{-}D10/E9}$ ("N40-D10-E9") or $OspC_{PBr}$ ("PBr"). After 21 days, *B. burgdorferi* genomes in the inoculation site, bladder, knee, ankle, heart and ear were enumerated by quantitative PCR (qPCR), which amplify this chromosomal gene (Fig 5A). As previously shown [28], mice infected with *ospC*-deficient B31-A3 had significantly (in this case, at least 35-fold) lower bacterial burden in all tissues examined compared to B31-A3/pBSV2G at 21 days post infection (d.p.i.)(Fig 5A, "B31-A3Δ*ospC*/Vector" vs. "B31-A3/Vector"). In fact, in 80–100% of tissue samples, *ospC*-deficient B31-A3 was below the limit of detection of 10 copies per 100ng of DNA. The colonization defect was due to the *ospC* mutation because the introduction of $pOspC_{B31}$ restored bacterial burdens back to wild type levels in all tissues (Fig 5A, "B31"). In addition, we found that B31-A3Δ*ospC* that ectopically produces $OspC_{N40\text{-}D10/E9}$, which promotes spirochetal binding to fibronectin in addition to dermatan sulfate (Fig 4), was capable of wild type levels of colonization in all tissues at 21 d.p.i. (Fig 5A, "N40-D10/E9"). The levels of bacteria in all of the tissues tested were 16- to 269-fold greater than that of B31-A3Δ*ospC* harboring vector alone and statistically indistinguishable from that of B31-A3 or B31-A3Δ*ospC*/$pOspC_{B31}$. Importantly, the pBSV2-derived *ospC*-encoding plasmids were retained *in vivo*, because at 21 day post infection, the copy number of these plasmids relative to chromosomal copy number for each of the colonizing strains in the tissues in which they were detected was roughly equivalent to the pBSV2 copy number of spirochetes cultivated *in vitro* with antibiotic selection (S3 and S4 Tables).

Although $OspC_{PBr}$ binds to fibronectin, in contrast to $OspC_{N40\text{-}D10/E9}$ and $OspC_{B31}$, it lacks the ability to efficiently bind to dermatan sulfate (Table 1). We found that, 21 days after inoculation, B31-A3Δ*ospC*/$pOspC_{PBr}$ was present at the inoculation site, bladder, heart and ear at levels indistinguishable from wild type B31-A3, indicating that this *B. garinii*-derived OspC retained colonization-promoting activity (Fig 5A, "PBr"). However, B31-A3Δ*ospC*/$pOspC_{PBr}$ was not found at high levels in either the knee or ankle at 21 days after inoculation. In both

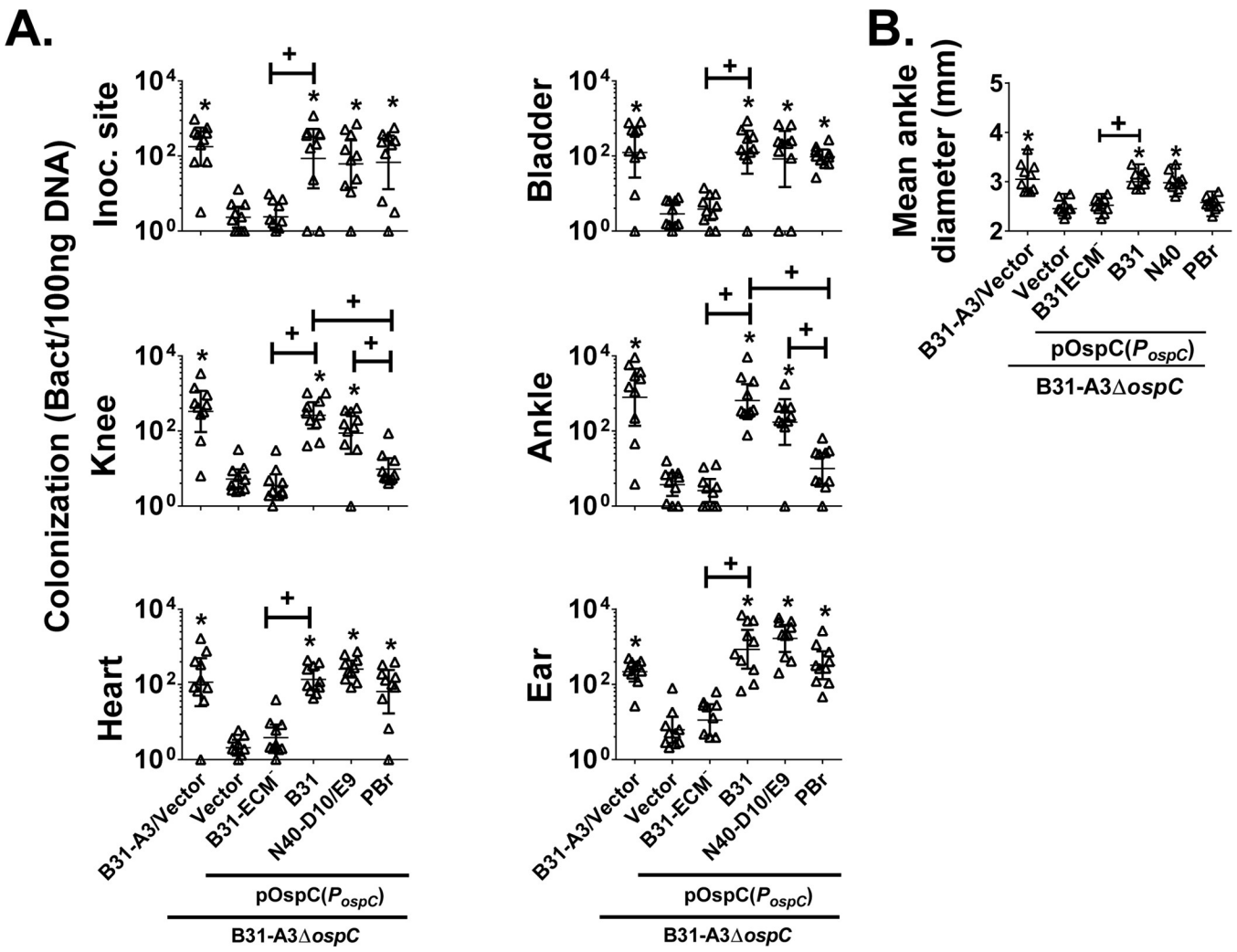

Fig 5. OspC variants promote distinct *B. burgdorferi* tissue colonization profiles at 21 days post infection. (A): C3H/HeN mice infected with 10^4 *B. burgdorferi* strain B31-A3/pBSV2G ("B31-A3/Vector"), *ospC*-deficient strain B31-A3Δ*ospC*/pBSV2G ("Vector"), or the deletion strain bearing a plasmid encoding the indicated OspC variants were euthanized at 21 days post infection. The bacterial loads at the inoculation site, ear, bladder, heart, knee, and ankle were determined by qPCR. Data shown are the geometric mean of bacterial loads ± 95% confidence interval of 10 mice per group. Statistical significance was determined using ANOVA with the Kruskal-Wallis test followed by the two-stage step-up method of Benjamini, Krieger and Yekutieli. Significant ($p < 0.05$) differences in spirochete number relative to the *ospC* deletion strain ("*") and between two strains relative to each other ("+") are indicated. **(B)** Joint diameter of mice infected with 10^4 of *B. burgdorferi* strain B31-A3/pBSV2G ("B31-A3/Vector"), *ospC*-deficient strain B31-A3Δ*ospC*/pBSV2G ("Vector"), or the deletion strain bearing a plasmid encoding the indicated OspC variants was measured by caliper on day 21 post infection. Data shown are the median of the diameter of ankle joints ± the range of these values in 10 mice per group. Statistical significance was determined using ANOVA with the Kruskal-Wallis test followed by the two-stage step-up method of Benjamini, Krieger and Yekutieli. Significant ($p < 0.05$) differences in the average diameter of ankle joint relative to the *ospC* deletion strain ("*") and between two strains relative to each other ("+") are indicated.

https://doi.org/10.1371/journal.ppat.1008516.g005

joints, the level of colonization of B31-A3Δ*ospC*/pOspC$_{PBr}$ was at least 64- to 9-fold (and significantly) lower than that promoted by either B31-A3Δ*ospC*/pOspC$_{B31}$ or B31-A3Δ*ospC*/OspC$_{N40\text{-}D10/E9}$, respectively, and only 1.8 to 2.7-fold higher than (and statistically indistinguishable from) B31-A3Δ*ospC*. Additionally, B31-A3Δ*ospC*/pOspC$_{PBr}$ could not be detected in 50% and 70% of knee and ankle samples, respectively. These results indicate that OspC$_{PBr}$ promotes colonization of several tissues but not the joints, consistent with the hypothesis that dermatan sulfate binding specifically promotes joint colonization.

To determine whether the inability of $OspC_{PBr}$ to promote long-term colonization of the ankle resulted in a change in a disease manifestation, i.e. joint swelling, we measured the diameters of the ankle joints just prior to euthanasia. Consistent with the lack of joint colonization at 21 days post infection, the diameters of the ankle joints of mice infected with B31-A3Δ*ospC*/pBSV2G (Fig 5B, "Vector") were significantly smaller than those of mice infected with either the wild type strain B31-A3/pBSV2G (Fig 5B, "B31-A3/Vector") or B31-A3Δ*ospC*/$pOspC_{B31}$ (Fig 5B, "B31"), both of which colonize this tissue at high levels. Mice infected with B31-A3Δ*ospC*/$OspC_{N40\text{-}D10/E9}$ also displayed ankle swelling similar to that caused by strain B31-A3 (Fig 5B, "N40-D10/E9"). Finally, consistent with the lack of detectable joint colonization by B31-A3Δ*ospC*/$OspC_{PBr}$ (Fig 5B, "PBr"), mice infected with these strains had ankle diameters that were not significantly different than those of mice inoculated with the *ospC*-deficient strain B31-A3Δ*ospC*/pBSV2G. Thus, only those OspC proteins that retained the ability to bind to dermatan sulfate ($OspC_{B31}$) or both dermatan sulfate and fibronectin ($OspC_{N40\text{-}D10/E9}$) were capable of promoting joint colonization and swelling in mice.

B. burgdorferi producing an OspC mutant incapable of binding ECM displays a dramatic colonization defect that is indistinguishable from that of an *ospC*-deficient strain

$OspC_{B31\text{-}ECM}^{-}$ lacks not only dermatan sulfate-binding activity, but also fibronectin-binding activity. To test whether the ability to promote colonization of any tissue during murine infection correlates with the ability to bind ECM components, we assessed infection by B31-A3Δ*ospC*/$pOspC_{B31\text{-}ECM}^{-}$. We found that this strain was unable to colonize any of the tissues at levels greater than the *ospC*-deficient mutant (Fig 5A; "B31-ECM^{-}"vs. "Vector"). Note that $pOspC_{B31}$ differs from $pOspC_{B31\text{-}ECM}^{-}$ (as well as from $pOspC_{N40\text{-}D10/E9}$ and $pOspC_{PBr}$) not only in the *ospC* coding sequence, but also in the eight nucleotides just 5' to the *ospC* ATG start codon. Thus, we generated B31-A3Δ*ospC*/$pOspC_{B31\ \#2}$, which carries the same eight nucleotide substitution 5' to the *ospC* coding sequence (S4A Fig, "B31-ECM^{-}"vs. "B31 #2"). At 21 days post infection, B31-A3Δ*ospC*/$pOspC_{B31\ \#2}$ but not B31-A3Δ*ospC*/$pOspC_{B31\text{-}ECM}^{-}$ was capable of colonization. As above, analysis of the relative copy number of $pOspC_{B31\ \#2}$ showed that the plasmid was retained during murine infection (S5 Table). As expected, a defect in colonization by B31-A3Δ*ospC*/$pOspC_{B31\text{-}ECM}^{-}$ corresponded to an absence of joint swelling (S4B Fig) or an anti-*B. burgdorferi* antibody response any greater than that triggered by a strain entirely lacking *ospC* (S5 Fig). This experiment also showed that the colonization defects of *B. burgdorferi* producing $OspC_{PBr}$ or $OspC_{B31\text{-}ECM}^{-}$ was not associated with differences in antibody response to these strains. Further, the tissue tropism of these strains was not altered upon infection of C3H/HeN-SCID mice, which are incapable of generating an adaptive immune response, indicating that the colonization defects of $OspC_{PBr}$ or $OspC_{B31\text{-}ECM}^{-}$ did not reflect differences in their ability to either elicit or evade the adaptive immune response (S6 Fig). Instead, these results indicate that the colonization defect of $OspC_{B31\text{-}ECM}^{-}$ was due to *ospC* coding sequence mutations that abolish ECM binding by this protein.

ECM-binding by OspC is required for vascular transmigration into joint tissue 24 hours after intravenous inoculation

To determine if OspC plays an essential role in *B. burgdorferi* transmigration into knee joint tissue, we used our previously developed 24-hour intravital vascular transmigration assay [62] using $Cd1d^{-/-}$ mice. These mice lack iNKT cells, which provide the primary innate immune response in the mouse joint [63, 64]. In the absence of iNKT cells, *B. burgdorferi* that transmigrates into joint tissue is not phagocytosed and can be counted one day after *i.v.* injection.

Mice were injected with *B. burgdorferi* strain B31-A3 or an *ospC*-deficient mutant in this strain background harboring the vector pTM61 expressing GFP, or the *ospC*-deficient mutant complemented with a plasmid encoding *ospC* from *B. garinii* PBr. The *ospC* coding region in this complementing plasmid was under the control of the *flaB* promoter (see S1 Table for strain information). Intravital microscopy using a spinning disk laser confocal microscope was performed at 24 hrs post-inoculation. Upon staining blood vessels with Alexa Fluor 647 anti-PECAM-1 antibody, images of the left knee to a depth of 200 μm were collected during the one hr intravital experiment. Spirochetes that had transmigrated into the tissue surrounding the knee were counted (Fig 6A). Compared with the wild type strain, a dramatic decrease in transmigration into the joint tissue was observed for the *ospC*-deficient strain. In spite of the fact that $OspC_{PBr}$ did not promote joint localization in the short-term infection model or joint colonization model, we found that complementation of the *ospC*-deficient strain with a plasmid that produces $OspC_{PBr}$ restored vascular transmigration (Fig 6B, "PBr").

A potential confounding factor in this experiment is the ability of OspC, by binding the complement component C4b, to promote bloodstream survival [43]. Indeed, we found here that the rate of clearance of the *ospC*-deficient spirochete was significantly faster compared with the wild type strain, and that complementation with an $OspC_{PBr}$–producing plasmid restored the wild type clearance rate in *Cd1d*$^{-/-}$ mice (Fig 6C). Thus, OspC could be directly involved in spirochete extravasation or, by protecting *B. burgdorferi* from clearance, indirectly promoting detectable levels of transmigration. Therefore, we assessed the transmigration of the $OspC_{B31\text{-}ECM}^{-}$ mutant, which we showed retains the abilty to bind C4b (S2D Fig). In contrast to the *ospC*-deficient *B. burgdorferi*, the strain producing $OspC_{B31\text{-}ECM}^{-}$ displayed a clearance rate almost identical with wild type *B. burgdorferi* strain B31-A3 harboring the vector (Fig 6D). Moreover, compared with wild type *ospC*$_{B31}$, the $OspC_{B31\text{-}ECM}^{-}$ mutant was entirely defective at transmigration into the knee (Fig 6E). Therefore, we conclude that OspC, in addition to protection from clearance, plays an essential role in *B. burgdorferi* vascular transmigration into joint tissue.

Discussion

Tissue colonization by multiple bacterial pathogens is a complex process that includes bloodstream survival, distinct and increasingly stable interactions with the vascular wall, and tissue invasion [8, 12]. *B. burgdorferi* OspC lipoprotein is upregulated while the bacteria are in the midgut of a feeding tick and is essential for the early stages of mammalian function [26, 28, 65, 66]. In addition, OspC is highly variable and distinct variants are associated with differences in strain invasiveness [32, 67, 68]. These observations have prompted several studies of its potential role in mammalian colonization [41–43, 69]. We recently found that OspC, by binding the complement component C4b, promotes bloodstream survival at early stages of infection [43]. Given that OspC of *B. burgdorferi* strain N40-D10/E9 was enriched for tissue localization upon i.v. inoculation of a phage display library [49], here we examined the role of OspC as a potential adhesin that influences tissue colonization by Lyme disease bacteria. We found that recombinant $OspC_{N40\text{-}D10/E9}$ binds to both dermatan sulfate and fibronectin and identified three functional OspC groups, typified by: (1) $OspC_{N40\text{-}D10/E9}$, which efficiently (i.e., $K_D \leq$ 0.8 μM by SPR) binds dermatan sulfate and fibronectin; (2) $OspC_{B31}$, which binds dermatan sulfate but not fibronectin; and (3) $OspC_{PBr}$, which binds fibronectin but not dermatan sulfate. Using a one-hour *i.v.* C3H mouse infection model that likely measures initial vessel wall adherence in different vascular beds, we found that $OspC_{N40\text{-}D10/E9}$ and $OspC_{B31}$, which both bind dermatan sulfate, were capable of promoting spirochetal localization to ankles when produced

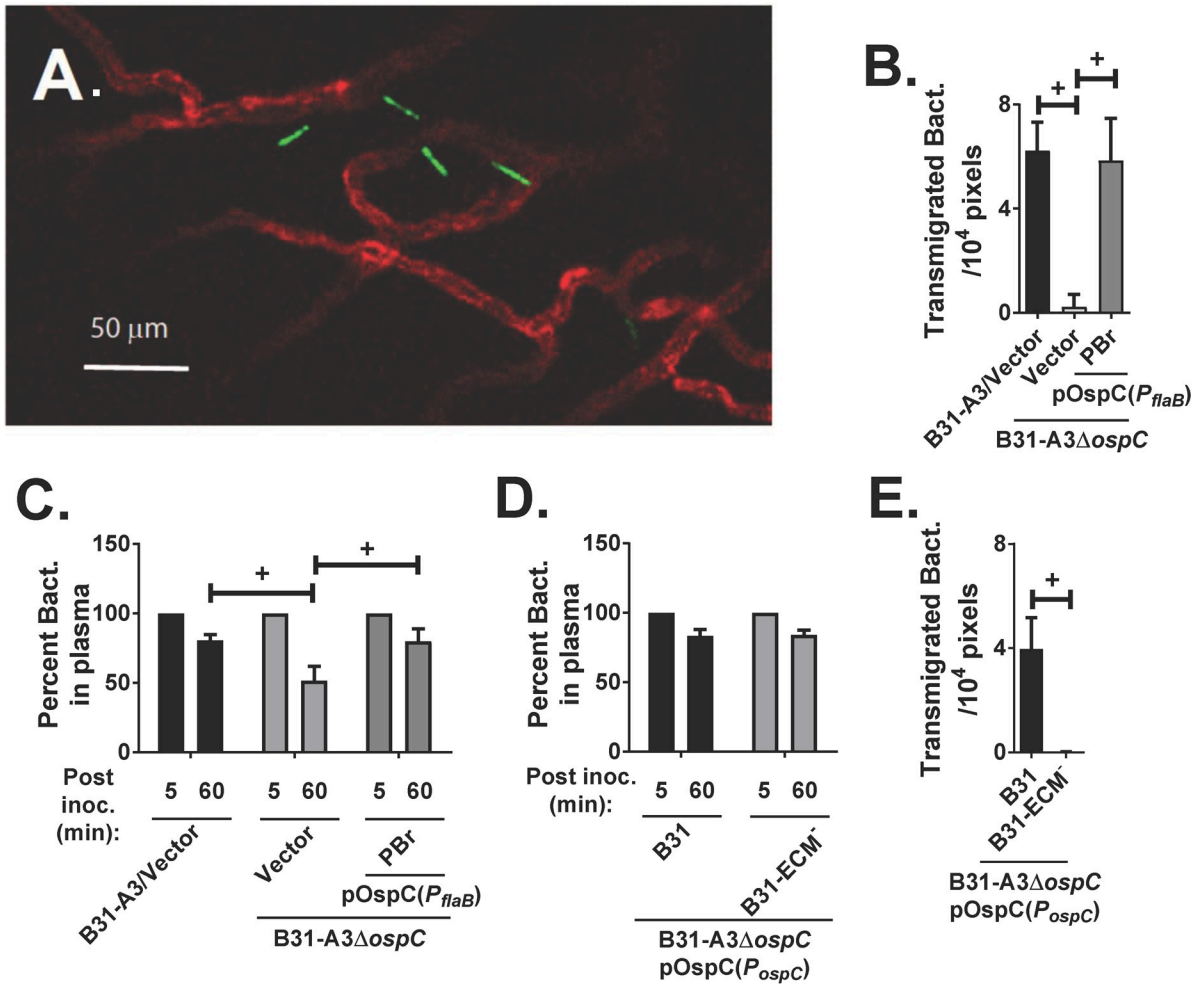

Fig 6. OspC is required for vascular transmigration in the knee of *Cd1d*$^{-/-}$ mice. (A) Image of transmigrated GFP-producing *B. burgdorferi* by intravital microscopy. Blood vessels were stained with Alexa Fluor 647 anti-PECAM-1 (CD31) antibody shown in red color. **(B)** Transmigration levels of GFP-expressing *B. burgdorferi* strains producing wild type $OspC_{B31}$ ("B31-A3/Vector", i.e. B31-A3/pTM61, GCB 847), no OspC ("Vector", i.e. B31-A3Δ*ospC*/pTM61spc, GCB 3007) and $OspC_{PBr}$ ("PBr", i.e. B31-A3Δ*ospC*/pTM61spc-$OspC_{PBr}$(P_{flaB}), GCB 3226). Spirochetes outside of the vasculature (n = 5 mice) were counted in total and plotted as the number of transmigrated spirochetes in an area of 10^4 pixels. Statistical significance was determined using ANOVA with the Kruskal-Wallis test followed by the two-stage step-up method of Benjamini, Krieger and Yekutieli. Significant ($p < 0.05$) differences in the levels of transmigrated bacteria between two strains relative to each other ("+") are indicated. **(C)** Clearance of *B. burgdorferi* from the vasculature. The change in spirochete concentration between 5 and 60 minutes was determined for each mouse as the percentage of spirochetes present at 60 minutes relative to the initial 5 minute time point. Statistical significance was determined using ANOVA with the Kruskal-Wallis test followed by the two-stage step-up method of Benjamini, Krieger and Yekutieli. Significant ($p < 0.05$) differences in the percent bacteria in plasma between two strains relative to each other ("+") are indicated **(D)** Spirochete clearance was analyzed for the experiments described in panel E as described in panel C. Statistical significance was determined using ANOVA with the Kruskal-Wallis test followed by the two-stage step-up method of Benjamini, Krieger and Yekutieli. Significant ($p < 0.05$) differences in the levels of transmigrated bacteria between two strains relative to each other ("+") are indicated. **(E)** Transmigration levels of GFP-expressing *B. burgdorferi* strains producing wild type $OspC_{B31}$ ("B31-A3/Vector", i.e. B31-A3Δ*ospC*/pTM61-$OspC_{B31}$(P_{ospC}), GCB 4458) or $OspC_{B31\text{-}ECM^-}$ ("B31-ECM$^-$", i.e. B31-A3Δ*ospC*/pTM61-$OspC_{B31\text{-}ECM^-}$(P_{ospC}), GCB 4452). *Cd1d*$^{-/-}$ mice were injected *via* the tail vein (n = 3 mice) with GFP-producing low-passage strains and transmigration levels were analyzed at 24 hrs as described above.

https://doi.org/10.1371/journal.ppat.1008516.g006

on the surface of an *ospC*-deficient *B. burgdorferi* strain. In contrast, $OspC_{PBr}$, which binds fibronectin but not dermatan sulfate, did not.

To test whether the fibronectin and dermatan sulfate adhesive activities of OspC are essential for long-term colonization, we first compared the sequences of OspC variants capable or

incapable of binding dermatan sulfate to identify a highly basic candidate GAG-binding region of α-helix 3 and loop 4, conserved in all of the OspC-displaying phage that promoted tissue localization in mice. Methionine substitution of five lysine residues in this region resulted in $OspC_{B31\text{-}ECM^-}$, which retains secondary structure but is incapable of recognizing either dermatan sulfate or fibronectin. We then tested isogenic strains that produce either $OspC_{B31}$ or $OspC_{B31\text{-}ECM^-}$ for the ability to colonize C3H mice after *i.d.* inoculation. We found that whereas wild type $OspC_{B31}$ promoted colonization of all tissues tested at three weeks post infection, the strain producing $OspC_{B31\text{-}ECM^-}$ was no more capable of colonization of any tissues than the control *ospC*-deficient strain. These results indicate that not only does OspC promote spirochetal binding to the ECM components, fibronectin or dermatan sulfate, but this adhesive activity is essential for mammalian infection.

Given that OspC displays strain-specific differences, we evaluated the role of such differences in long-term colonization of mammalian tissues. Upon *i.d.* inoculation of C3H mice with isogenic *B. burgdorferi* strains that differ only in their *ospC* coding sequence, we found that the $OspC_{N40\text{-}D10/E9}$, $OspC_{B31}$, and $OspC_{PBr}$, each of which binds fibronectin, dermatan sulfate, or both, were fully capable of promoting colonization of the injection site, ear, heart and bladder at three weeks post infection. However, only those variants capable of binding dermatan sulfate, i.e. $OspC_{N40\text{-}D10/E9}$ and $OspC_{B31}$, were able to promote colonization of the knee and ankle joints; joint colonization by the strain producing $OspC_{PBr}$ was no greater than an *ospC*-deficient mutant. These results suggest that dermatan sulfate binding by OspC is required for joint colonization.

Lyme disease spirochetes encode a plethora of GAG-binding adhesins, including BBK32, DbpA and DbpB, which bind dermatan sulfate, Lmp1 and Bgp, which bind chondroitin-6-sulfate, and OspF protein family members, which bind heparan sulfate [54–57, 59, 70]. The dermatan sulfate-binding activity of DbpA is essential for colonization of multiple tissues [21, 22] whereas that activity of BBK32 promotes joint colonization [20]. *B. burgdorferi* producing mutants of OspC, BBK32 or DbpA specifically defective for dermatan sulfate binding demonstrate colonization defects, indicating that these GAG-binding activities, which are of roughly comparable affinity (K_Ds of 0.21 to 0.91 μM) when evaluated with purified substrates [20, 22], function in a non-redundant fashion during colonization. Presumably, this non-redundancy reflects differences in adhesin-mediated GAG-binding activities that have not yet been discerned and a tissue colonization process that requires the sequential or simultaneous action of each of these activities.

The association of strain invasiveness with *ospC* type could reflect direct involvement of the OspC protein in tissue tropism, or could simply be a genetic marker of spirochetal strains that encode non-*ospC* tropism determinants [67, 68]. Our analyses of isogenic strains revealed that the OspC variant produced by a Lyme disease strain is in fact a direct determinant of the strain's tissue tropism; in fact variants derived from *B. burgdorferi* sensu stricto, a species that is associated with human Lyme arthritis [3], promote greater joint colonization and more severe disease in the C3H mouse than variants produced by 'non-arthritogenic' species of Lyme spirochete. An attractive model is that a complex spectrum of GAG-binding activities conferred by variable adhesins such as OspC, DbpA or members of the OspF family contributes to observed differences in tissue tropism by different strains during human Lyme disease [22, 56]. Of note, OspC is a critical determinant of the early stage infectivity of *B. burgdorferi*, when the bacteria are establishing infection and actively disseminating from the site of the tick bite.

Dermatan sulfate GAGs are found in the vascular bed of joints [71]. The ability of $OspC_{N40\text{-}D10/E9}$ and $OspC_{B31}$ to foster localization to ankles 60 minutes after *i.v.* inoculation suggests that these dermatan sulfate-binding proteins promote initial interaction with joint

vasculature. The finding that $OspC_{N40\text{-}D10/E9}$ and $OspC_{B31}$ each promoted joint colonization three weeks after i.d. inoculation raised the possibility of a function in tissue invasion subsequent to early vascular attachment. Intravital microscopy was used to quantify joint invasion 24 h after i.v. infection of *Cd1d*$^{-/-}$ BALB/c mice with GFP-producing strains provided a direct means to interrogate a role for OspC in joint tissue invasion. We found that a strain producing $OspC_{PBr}$ enters joints far more efficiently than an *ospC*-deficient strain. This result was not predicted from our finding that this variant was not capable of promoting joint localization one hr after i.v. infection or joint colonization three weeks after i.d. inoculation and suggests the possibility that although $OspC_{PBr}$ is fully functional in promoting vascular transmigration, it may nonetheless be compromised in an earlier, presumably distinct step of the dissemination cascade [72–74] [75]. However, direct comparison of the three types of murine infection assays is confounded by differences in several experimental parameters, including *B. burgdorferi* and murine strain background, control of *ospC* expression, and route and duration of infection. Moreover, assessing whether $OspC_{PBr}$ directly participated in the movement of bacteria from the bloodstream into the joint was complicated by the fact that this protein, as predicted by previous studies [18, 43], enhanced spirochetemia in *Cd1d*$^{-/-}$ BALB/c mice. Thus, we instead compared isogenic strains that produced either $OspC_{B31}$, which binds dermatan sulfate, or $OspC_{B31\text{-}ECM}^{-}$, which does not. $OspC_{B31\text{-}ECM}^{-}$ retained the ability to bind C4b and promoted bloodstream survival in *Cd1d*-deficient mice indistinguishably from $OspC_{B31}$, allowing a straightforward comparison of joint invasion promoted by the two proteins. This comparison revealed a direct role of the OspC adhesive activity in joint invasion.

Combined with previous work defining the role of several *B. burgdorferi* adhesins in the tissue invasion process, an emerging model is that movement of the spirochete from the bloodstream into tissue is a multistep process mediated by a series of adhesive events [8, 12]. The fibronectin-binding activity of BBK32 promotes an initial 'tethering' interaction with the vascular wall through catch-bond interactions under shear stress, and its dermatan sulfate-binding activity promotes the more stable 'dragging' interaction [9, 50, 76, 77]. Thereafter, integrin-binding by the *B. burgdorferi* outer membrane protein P66 is essential for joint invasion [62]. Here we showed a critical role for dermatan sulfate-binding by OspC for vascular transmigration. As is the case for P66-endothelial interactions, the interaction of OspC with the vascular endothelium leading to extravasation appears to occur subsequent to early tethering and dragging interactions that decelerate the spirochetes under the shear stress of bloodflow, because the presence of OspC does not impart detectable tethering or dragging interactions in the absence of both BBK32 and VlsE, powerful adhesins that promote deceleration under shear flow [Tan, X. et al, manuscript in preparation]. The molecular mechanism by which OspC promotes vascular transmigration remains unknown at this time, but it is tempting to speculate that it may induce endothelial signaling to promote cellular changes required for spirochetal transmigration. Nonetheless, a direct role of OspC in transmigration subsequent to deceleration certainly does not preclude earlier role(s) in survival and the tissue colonization pathway. The emerging picture is that OspC is a multifunctional protein with crucial roles in the pathogenesis process.

Invasion of mammalian leukocytes into tissues during the inflammatory process features several parallels, as it is well-documented to occur via a multi-step process involving counter-receptors for both lectins and integrins [78, 79]. Given these conserved themes, it seems likely that the observed tropism of other species of Lyme disease for non-joint tissues such as skin, heart or neural tissue may result from the sequential action of alternate sets of bacterium-host cell interactions. Similar multi-faceted analyses of isogenic strains of such Lyme disease species that vary in their repertoire of adhesive surface factors, such as the study described here, is an important goal. With the with further development of genetic techniques in these species, as

well as the development of small animal models that reflect human tropism, such studies will provide rigorous means to identify and characterize these interactions and to better understand the molecular basis underlying diverse tissue tropisms characteristic of different Lyme disease spirochetes.

Materials and methods

Ethics statement

All mouse experiments were performed in strict accordance with all provisions of the Animal Welfare Act, the Guide for the Care and Use of Laboratory Animals, and the PHS Policy on Humane Care and Use of Laboratory Animals. The protocol was approved by the Institutional Animal Care and Use Committee (IACUC) of Medical College of Wisconsin, Tufts University School of Medicine, Wadsworth Center-New York State Department of Health, or University of Calgary. All efforts were made to minimize animal suffering.

Animals

Female C3H/HeN or C3H/HeN-SCID mice were acquired from Charles River Laboratories (Charles River Laboratories International, Inc., Wilmington, MA) and used at 4 wks of age for long term intradermal inoculation studies, or 8 wks of age or older for short term intravenous (i.v) inoculation experiments. For intravital microscopy *Cd1d*$^{-/-}$ mice in a BALB/c background (Jax #2962) were bred in-house at the Clara Christie Centre for Mouse Genomics at the University of Calgary. Mice of both genders between 6–8 weeks of age were used.

Bacterial strains and culture conditions

All strains used in this study are described in S1 Table. *B. burgdorferi* strains were grown in Barbour-Stoenner-Kelly (BSKII) medium made in-house [80] containing 6% rabbit serum at 33˚C to a density of 1x10^8 spirochetes/ml. When antibiotic selection was required, kanamycin was used at 200 μg/ml and gentamicin was used at 40 μg/ml. Presence of genomic plasmids and shuttle vectors was confirmed in each culture by PCR prior to inoculation into mice (S2 Table) [81–83]. *Escherichia coli* strains DH10B, BL21 and their derivatives (S1 Table) were grown in Luria-Bertani broth (BD Bioscience, Franklin Lakes, NJ) or agar supplemented with ampicillin (100 μg/ml) when necessary.

Strain construction

The *ospC*-deficient *B. burgdorferi* strain B31-A3 (OspCK1), generated previously [28], was engineered to express o*spC* alleles from various strains and species of *Borrelia* from the *ospC* promoter and ribosome binding site from strain B31-A3, or constitutively from the flagellar promoter (*flaB*) and ribosome binding site native to each *ospC* allele [43], in pBSV2G (S1 Table). This strain as background in this study because of the available genetic tools and information (plasmid profiles) and small animal models that can apply to this strain. To express $ospC_{B31}$ under control of the $OspC_{B31\text{-}A3}$ promoter, 200bp upstream of the start codon of $ospC_{B31\text{-}A3}$ with the coding sequences of $ospC_{B31}$ were cloned into pBSV2G, resulting in $pOspC_{B31}$ [28]. For expression of $ospC_{N40\text{-}D10/E9}$, $ospC_{PBr}$, or $ospC_{B31\text{-}ECM}^{-}$ under control of the $ospC_{B31\text{-}A3}$ promoter, *ospC* alleles were amplified using primers (S2 Table) containing SalI and BamHI sites at the 5'and 3' ends, respectively, from genomic DNA isolated from *B. burgdorferi* strains B31-A3 and N40-D10/E9, and *B. garinii* strain PBr using the Wizard SV Genomic DNA Purification System (Promega corp., Madison, WI). Amplified DNA fragments were inserted into the TA cloning vector, pGEM-T Easy (Promega corp.). To generate pGEM-T

Easy encoding $OspC_{B31\text{-}ECM}^{-}$, site-directed, ligase-independent mutagenesis (SLIM) was used to replace lysines-116, 121, 123, 128, and 129 of OspC from *B. burgdorferi* strain B31-A3 with methionines on pCR2.1 TOPO encoding $OspC_{B31\text{-}A3}$ as described [84]. Those pGEM-T Easy-derived plasmids encoding $ospC_{N40\text{-}D10/E9}$ or $ospC_{PBr}$, $ospC_{B31\text{-}ECM}^{-}$, were then digested with SalI and BamHI and *ospC* alleles were subcloned into pBSV2G at the SalI and BamHI sites [85]. The promoter region of *ospC* from *B. burgdorferi* B31-A3, 184 bp to 9 bp upstream of the start codon of *ospC* [54], was also PCR amplified, adding HindIII and SalI sites at the 5'and 3' ends, respectively, using primers pospCfp and pospCrp (S2 Table), resulting in plasmids $pOspC_{N40\text{-}D10/E9}$, $pOspC_{PBr}$, and $pOspC_{B31\text{-}ECM}^{-}$. Note that $pOspC_{B31}$ differs from $pOspC_{B31\text{-}ECM}^{-}$ (as well as from $pOspC_{N40\text{-}D10/E9}$ and $pOspC_{PBr}$) not only in the *ospC* coding sequence, but also in the eight nucleotides just 5' to the *ospC* ATG start codon. We thus also generated $pOspC_{B31\ \#2}$ with the same nucleotides 5' to the *ospC* ATG start codon (S1 Text).

To generate strains to be utilized in short-term *i.v.* infections, genomic DNA was isolated from *B. burgdorferi* strain B31-A3 and N40-D10/E9, and *B. garinii* strain PBr using the Wizard SV Genomic DNA Purification System (Promega corp., Madison, WI). *ospC* alleles containing the native ribosome binding sites (which were identical) were amplified from genomic DNA using the oligonucleotides described in S2 Table. PCR fragments containing the *ospC* alleles were cloned in pGEM-T Easy (Promega corp., Madison, WI). Plasmid pTM61spc-MCS was generated by annealing oMCS3 and oMCS4 and ligating the fragment into pGEM-T Easy. The MCS was excised from pGEM-T Easy (Promega corp., Madison, WI) using *Bsp*HI and *Ear*I, and ligated in pTM61spc [62] at the BspHI site. The flagellar promoter was amplified from *B. burgdorferi* strain B31-A3 genomic DNA using P-FlaB oligonucleotides (S2 Table), ligated in pGEM-T Easy (Promega corp., Madison, WI), excised using NheI and SalI (NEB, Ipswich, MA), and subcloned in the NheI and XhoI sites of pTM61spc-MCS (S1 Table). The *ospC* alleles in pGEM-T Easy were excised from the vector using SacI and XmnI (New England Bio-Labs, Inc., Ipswich, MA), and cloned downstream of the *flaB* promoter in pTM61spc-MCS (S1 Table). The *flaB* promoter-*ospC* allele fragments were excised from pTM61spc-MCS using *Hind*III and *Bam*HI and ligated in pBSV2G [28] at the HindIII/BamHI sites.

To generate GFP-producing *B. burgdorferi* strains, the *ospC*-deficient *B. burgdorferi* strain B31-A3Δ*ospC* (OspCK1) [28] was engineered to express *ospC* alleles under the control of the constitutive flagellar promoter (P_{flaB}) in pTM61spc-MCS as previously described [43] or under the control of the native *ospC* promoter in pBSV2G (S1 Table). To build the complementing strains GCB4458 (B31-A3Δ*ospC*/pTM61-$OspC_{B31}$(P_{ospC})) and GCB4452 (B31-A3Δ*ospC*/pTM61-$OspC_{B31\text{-}ECM}^{-}$($P_{ospC}$)) with *ospC* under the control of the *ospC* promoter in pTM61, the wild type ($ospC_{B31}$) and mutated ($ospC_{B31\text{-}ECM}^{-}$) genes were first subcloned in pJET1.2 (ThermoScientific, Waltham, MA). To do so, both genes were amplified by using $OspC_{B31}$fp/pTM61 and $OspC_{B31}$rp/pTM61, including restriction sites for SbfI and AvrII respectively (S2 Table). The DNA used as template for the wild type $ospC_{B31}$ under the control of the *ospC* promoter was $pOspC_{B31}$(P_{ospC}), while $ospC_{B31\text{-}ECM}^{-}$ controlled by the *ospC* promoter was amplified from $pOspC_{B31\text{-}ECM}^{-}$($P_{ospC}$). Each insert was ligated into pJET1.2.Plasmids pTX4 (pJET::$ospC_{B31}$), pTX5 (pJET::$ospC_{B31\text{-}ECM}^{-}$) and pTM61 were double digested with the restriction enzymes SbfI and AvrII, acquired from NEB. Digestions were run in a 1% agarose gel and the bands corresponding to pTM61 (6.7 Kb), $ospC_{B31}$ (817bp) and $ospC_{B31\text{-}ECM}^{-}$ (817bp) were gel purified. Ligations were performed to obtain plasmids pMC114 (pTM61::$ospC_{B31}$) and pMC115 (pTM61::$ospC_{B31\text{-}ECM}^{-}$). The resulting constructs were sequenced with oligos $OspC_{B31}$fp/pTM61 and $OspC_{B31}$rp/pTM61 to confirm their integrity. Strains GCE3815 ($ospC_{B31}$) and GCE3817 ($ospC_{B31\text{-}ECM}^{-}$) were grown overnight in LB to purify the respective plasmids pMC114 and pMC115 by midiprep (Qiagen, Germantown, MD). 150 μg of plasmids pMC114 and pMC115 were incubated individually with the GpC

methyltransferase M.CviPI according to NEB protocols. After precipitation with isopropanol followed by 70% ethanol, 50 μg of each plasmid was transformed into electrocompetent strain B31-A3Δ*ospC* (GCB3022). Candidate transformants were screened for the presence of the gentamicin cassette and the *ospC* insert, either wild type ($ospC_{B31}$) or ECM mutant ($ospC_{\text{B31-ECM}^-}$). They were also tested for green fluorescence (GFP harbored in pTM61). Finally, the plasmid profiles were analyzed as reported [81]. The strain complemented with the wild type *ospC* version lost lp28-4 and lp56. However, these plasmids have not been shownto affect infectivity [83]. The final strains (S1 Table) were GCB4458 (B31-A3Δ*ospC*/pTM61-$OspC_{B31}$(P_{ospC})) and B31-A3Δ*ospC*/pTM61-$OspC_{\text{B31-ECM}^-}$(P_{ospC}) (GCB4452).

Plasmid constructs in *E. coli* were isolated using the QIAGEN Plasmid Maxi Kit (Qiagen, Valencia, CA) and transformed into *B. burgdorferi* by electroporation of 50 μg of CpG methylated DNA and plating into semi-solid agar or in liquid in 96-well plates as previously described [24, 86]. All *ospC* alleles were found to have the correct sequence when carried on pBSV2G or pTM61 in *B. burgdorferi* with the exception of the *ospC* allele from *B. burgdorferi* strain N40-D10/E9, which was found to encode the single missense mutation N46S after multiple independent PCR amplifications [43]. The quantitation of surface exposure of the resulting strains is described in S1 text.

Recombinant GST-fusion proteins

To generate recombinant GST-tagged OspC proteins, the *ospC* open reading frames lacking the putative cleaved signal sequences from *B. burgdorferi* strains B31-A3, 297, and N40-D10/E9, *B. garinii* strain PBr, *B. afzelii* strain VS461, and an altered open reading frame encoding $OspC_{\text{B31-ECM}^-}$ (lysine residues 116, 121, 123, 128, and 129 were replaced with methionines) were amplified (S2 Table) and cloned into pGEX4T2 at the BamHI and SalI sites (GE Healthcare, Piscataway, NJ), as previously described [24, 43]. Plasmids were transformed into *E. coli* strain BL21(DE3) and the plasmid inserts were sequenced (Tufts core sequencing facility). The GST-tagged OspC variants were produced and purified by glutathione chromatography according to the manufacturer's instructions (BD Bioscience, Franklin Lakes, NJ).

Glycosaminoglycan and fibronectin binding assays

Quantitative ELISA for fibronectin and dermatan sulfate binding by OspC proteins was performed as previously described [87] with the following adjustments. To coat the wells with fibronectin and dermatan sulfate, these wells were incubated with 10 μg/ml of purified fibronectin or dermatan sulfate in the coating buffer (0.05 M Na_2CO_3, pH 9.0). One hundred microliters of increasing concentrations (0.03125, 0.0625, 0.125, 0.25, 0.5, 1, 2 μM) of GST (negative control) or GST-tagged OspC variants, including $OspC_{B31}$, $OspC_{297}$, $OspC_{N40\text{-}D10/E9}$, $OspC_{VS461}$, $OspC_{PBr}$, or $OspC_{\text{B31-ECM}^-}$ were added to the coated wells and incubated for 1 hr at ambient temperature. To detect the binding of GST-tagged proteins, goat anti-GST (Sigma-Aldrich, St. Louis, MO; 1:200) and HRP-conjugated donkey anti-goat IgG (Promega, Fitchburg, WI; 1:1,000) were used as primary and secondary antibodies, respectively. The plates were washed three times with PBST (0.05% Tween20 in PBS buffer), and 100 μl of tetramethyl benzidine (TMB) solution (KPL, Gaithersburg, MD) was added to each well. The reaction was stopped by adding 100 μl of 0.5% hydrosulfuric acid to each well and plates were read at 405 nm using a Synergy HT ELISA plate reader (BioTek, Winooski, VT). To determine the dissociation constant (K_D), the data were fit to the following equation using KaleidaGraph software

(Version 4.1.1 Synergy Software, Reading, PA).

$$OD405 = \frac{\text{OD405max[OspC proteins]}}{K_D\ \text{[OspC proteins]}}$$

Surface Plasmon Resonance (SPR)

Interactions of OspC with fibronectin or dermatan sulfate were analyzed by SPR using the Biacore 3000 (GE Healthcare, Piscataway, NJ). To conjugate SPR chips with fibronectin or dermatan sulfate, 10 μg of fibronectin in 10 μl of acetate buffer (CH_3COONa, pH 4.0) was flowed through a CM5 chip (GE Healthcare, Piscataway, NJ) whereas 10 μg of dermatan sulfate in 10 μl of PBS buffer was biotinylated as described [24] and flowed through an SA chip (GE Healthcare). A control flow cell was injected with PBS buffer without fibronectin or dermatan sulfate. For quantitative SPR experiments to determine fibronectin- or dermatan sulfate–binding, 10 μl of increasing concentrations (0, 15.625, 31.25, 62.5, 125, 250, 500 nM) of OspC variants including $OspC_{B31}$, $OspC_{297}$, $OspC_{N40\text{-}D10/E9}$, $OspC_{VS461}$, $OspC_{PBr}$, or $OspC_{B31\text{-}ECM^-}$, were injected into the control cell followed by the flow cell with immobilized fibronectin or dermatan sulfate at 10 μl/min, 25˚C. To obtain the kinetic parameters of the interaction, mean sensogram data were fit to a curve using BIAevaluation software version 3.0 (GE Healthcare, Piscataway, NJ) with the one step biomolecular association reaction model (1:1 Langmuir model), resulting in optimum mathematical fit with the lowest Chi square values.

Binding of radiolabeled *B. burgdorferi* to purified fibronectin and dermatan sulfate

Binding of *B. burgdorferi* to purified fibronectin or dermatan sulfate was determined essentially as previously described [24]. Briefly, spirochetes were radiolabeled with [^{35}S] methionine, and 1 x 10^8 radiolabeled bacteria were added to microtiter plate wells previously incubated with 250 μg/ml purified fibronectin, dermatan sulfate or BSA (negative control). After 1 hr at 37˚C, unbound bacteria were removed by washing with PBS containing 0.2% BSA. Plates were air-dried, and bound bacteria in each well were quantified by liquid scintillation. The percent of bound bacteria was calculated by normalizing the counts of each well to the counts in the inoculum.

Mouse infections

Four-week-old female C3H/HeN or C3H/HeN-SCID mice were infected by intradermal injection with 1X10^4 *B. burgdorferi* strain B31-A3/pBSV2G, an *ospC*-deficient *B. burgdorferi* strain B31-A3Δ*ospC*/pBSV2G, or B31-A3Δ*ospC* carrying a plasmid encoding $ospC_{B31}$, $ospC_{N40\text{-}D10/E9}$, $ospC_{PBr}$, or $ospC_{B31\text{-}ECM^-}$ driven by the B31-A3 *ospC* promoter (S2 Table). Mice were euthanized at 21 d.p.i. and the skin at the inoculation site, knee, ankle, bladder, heart, and ear were isolated. DNA was extracted from these tissues using the DNeasy Blood & Tissue kit (Qiagen, Valencia, CA). *B. burgdorferi* genomes in each tissue were quantified by qPCR (S2 Table) using a CFX Connect Real-Time PCR detection system (BioRad, Hercules, CA) in conjunction with SYBR green PCR Mastermix (BioRad, Hercules, CA) (95.0˚C for 5min, 94.0˚C for 1 sec, 66˚C for 15 sec repeated 45 times) [88]. The number of *recA* copies was calculated by first establishing a Ct standard curve using known amounts of the *recA* gene extracted from *B. burgdorferi* strain B31-A3. Genome numbers in each sample were derived by comparison to the standard curve.

The short term *i.v.* inoculation experiments were performed as described [18, 43]. C3H/HeN mice under anesthesia were inoculated retro-orbitally with $1x10^8$ *B. burgdorferi* cells in 100 μl. After 1 hr, blood was collected by cardiac puncture, and the mice were perfused with sterile saline to wash away any unbound bacteria from the vasculature. Tissues were harvested and DNA isolated for quantitation of *Borrelia* and mouse genomes by qPCR [18, 43].

Evaluation of joint swelling

C3H/HeN mice were intradermally inoculated with $1X10^4$ *B. burgdorferi* strain B31-A3 carrying the empty vector, B31-A3Δ*ospC* carrying the empty vector, or $ospC_{B31}$, $ospC_{N40\text{-}D10/E9}$, $ospC_{PBr}$, *or* $ospC_{B31\text{-}ECM}^{-}$complemented strains. Mice were examined for swelling of the ankles on 21 d.p.i. as described previously [89]. Ankles from the rear legs of each mouse were measured using a high precision metric caliper in a blinded fashion. The thickest diameters of the ankles were measured in each mouse, and the data are presented as the median diameter of ankles ± the range, n = 10.

Intravital vascular transmigration assays

For vascular transmigration assays, the deeply anesthetized $Cd1d^{-/-}$ mice were intravenously inoculated with spirochetes 24 hrs before imaging as described previously [62]. A GFP-producing low-passage, infectious, *B. burgdorferi* strain was injected into the tail vein of $Cd1d^{-/-}$ mice (4×10^8 spirochetes per mouse). At 24 hrs post spirochete injection, vascular transmigration was scored in the knee to a depth of about 150 microns in the living mice by intravital microscopy using a spinning disk laser confocal microscope. The area exposed was over the patellar ligament and to the medial side of the right hind limb. We examined post-capillary venules that drain blood from the anterior tibialis muscle and joint with the anterior tibial vein that drains into the great saphenous vein (see [62] for further details). Blood vessels were stained with Alexa Fluor 647 anti-PECAM-1 (CD31) antibody indicated in red color. The total spirochete number and the surgical area were determined using Adobe Photoshop CC (San Jose, CA) for calculation of the number of spirochetes per area (10^4 pixels). For spirochete clearance assays on mice used for intravital microscopy, blood was withdrawn from mice at 5 and 60 minutes post-inoculation. Blood cells were allowed to settle overnight in a heparinized capillary tube and spirochetes in the plasma were directly counted by dark-field microscopy [62].

Statistical analysis

Statistical analyses were performed using the Mann-Whitney unpaired t-test or ANOVA using the Kruskal-Wallis test followed by the two-stage step-up method of Benjamini, Krieger and Yekutieli using GraphPad Prism 7 as indicated in each figure legend. All qPCR data were log transformed prior to analysis. A P-value < 0.05 was considered significant. The data represent the median ± range, mean ± standard deviation, mean ± SEM, geometric mean ± 95% confidence interval, or geometric mean ± geometric standard deviation as indicated in each figure.

Supporting information

S1 Fig. OspC class protein sequence alignment. ClustalW alignment performed on protein sequences of OspC from *B. burgdorferi* (Bb) strain B31 ("Bb B31"), 297 ("Bb 297"), and N40-D10/E9 ("Bb N40-D10/E9"), *B. afzelii* strain VS461 ("Ba VS461"), and *B. garinii* strain PBr ("Bg PBr") using BioEditor Sequence Alignment Editor [90]. At each position, conserved amino acids are highlighted in black and similar amino acids are highlighted in grey. Asterisks

indicate $OspC_{B31}$ lysines that were mutated to methionines to abrogate ECM binding, resulting in $OspC_{B31\text{-}ECM^-}$. The fragment of OspC from N40-D10/E9 selected for binding to joint and heart by phage display [49] is underlined.
(TIF)

S2 Fig. Mutation of lysine residues 116, 121, 123, 128, and 129 of $OspC_{B31}$ does not affect its structure or ability to bind C4b. (A) The location of the quintuple basic residues (K116, K121, K123, K128, K129) mutated in $OspC_{ECM^-}$ mapped onto the crystal structure of $OspC_{B31}$ [91, 92]. Helix 3 and loop 4 are highlighted in blue and green, respectively. (B) Amino acid sequence alignment of helix 3 and loop 4 of different *ospC* alleles. "*" indicates residues mutated in $OspC_{B31\text{-}ECM^-}$. (C) Far-UV CD analysis of $OspC_{B31}$ and $OspC_{B31\text{-}ECM^-}$. The molar ellipticity, Φ, was measured from 190 to 250 nm for 10 μM of each protein in Tris buffer (pH7.5). (D) The indicated concentrations of GST, GST-$OspC_{B31}$, or GST-$OspC_{B31\text{-}ECM^-}$ were added to quadruplicate wells coated with human C4b, and binding (± standard deviation) was measured by ELISA (see Experimental Procedures). Shown is a representative of three independent experiments. The K_D values obtained from the average of three independent experiments were calculated and shown in the inset.
(TIF)

S3 Fig. OspC variants are produced on the surface of an infectious *B. burgdorferi* strain. **(A)** Flow cytometry analysis of OspC localized to the surface of parental strain *B. burgdorferi* B31-A3/pBSV2G ("B31-A3/Vector"; red), *ospC* deletion strain B31-A3Δ*ospC*/pBSV2G ("B31-A3Δ*ospC*/Vector"; orange), and the *ospC* deletion strain bearing a plasmid encoding $OspC_{B31}$ ("B31-A3Δ*ospC*/p$OspC_{B31}$"; blue). **(B)** OspC (top) or flagellin (bottom) on the surface of the indicated untreated (solid bars) or methanol-permeabilized (open bars) strains was quantitated by flow cytometry after staining with anti-OspC or anti-flagellin, respectively (see Materials and Methods). Values shown are relative to the production levels of OspC or flagellin on the surface of permeabilized *B. burgdorferi* strain B31-A3 harboring the empty vector. Each bar represents the mean of four independent determinations ± SEM. (*): indicates that surface production of the indicated proteins was significantly lower (* = $P < 0.05$, ANOVA with the Kruskal-Wallis test followed by the two-stage step-up method of Benjamini, Krieger and Yekutieli) than the detected production of OspC or Flagellin by *B. burgdorferi* strain B31-A3 harboring the vector.
(TIF)

S4 Fig. The colonization defect of OspC-ECM^- is due to the alteration of coding sequence. **(A)** C3H/HeN mice infected with 10^4 *B. burgdorferi* strain B31-A3/pBSV2G ("B31-A3/Vector"), *ospC* deletion strain B31-A3Δ*ospC*/pBSV2G ("Vector"), or the deletion strain bearing a plasmid encoding either $OspC_{B31\text{-}ECM^-}$ or $OspC_{B31\ \#2}$, which differ only in the *ospC* coding sequence, were sacrificed at 21 days post infection. The bacterial loads at the inoculation site, ear, bladder, heart, knee, and ankle joint were determined by qPCR. Data shown are the geometric mean of bacterial loads ± 95% confidence interval of 10 mice per group. Statistical significance was determined using ANOVA with the Kruskal-Wallis test followed by the two-stage step-up method of Benjamini, Krieger and Yekutieli. Significant ($p < 0.05$) differences in spirochete number relative to the *ospC* deletion strain ("*") and between two strains relative to each other ("+") are indicated. **(B)** Joint diameter of the mice infected with 10^4 of *B. burgdorferi* strain B31-A3/pBSV2G ("B31-A3/Vector"), *ospC* deletion strain B31-A3Δ*ospC*/pBSV2G ("Vector"), or the deletion strain bearing a plasmid encoding either $OspC_{B31\text{-}ECM^-}$ or $OspC_{B31\ \#2}$ was measured by caliper on day 21 post infection. Data shown are the median of the diameter of ankle joints ± the range of these values in five mice per group. Statistical significance was determined using ANOVA with the Kruskal-Wallis test followed by the two-stage step-up method of Benjamini, Krieger and Yekutieli. Significant

($p < 0.05$) differences in the average diameter of ankle joint relative to the *ospC* deletion strain ("*") and between two strains relative to each other ("+") are indicated.
(TIF)

S5 Fig. *B. burgdorferi* producing $OspC_{PBr}$ triggers an adaptive immune response indistinguishable from a strain producing $OspC_{B31}$ or $OspC_{N40\text{-}D10/E9}$, and *B. burgdorferi* producing OspCB31-ECM- triggers a response indistinguishable from an *ospC*-deficient strain. Serum titers of IgG (top panel) and IgM (bottom panel) of C3H/HeN mice infected with 10^4 *B. burgdorferi* strain B31-A3/pBSV2G ("B31-A3/Vector"), *ospC* deletion strain B31-A3Δ*ospC*/pBSV2G ("Vector"), or the *ospC* deletion strain bearing a plasmid encoding the indicated OspC variants sacrificed at 21 days post infection. Shown are the geometric mean of antibody titers ± 95% confidence interval of 10 mice per group. Statistical significance was determined using ANOVA with the Kruskal-Wallis test followed by the two-stage step-up method of Benjamini, Krieger and Yekutieli. Significant ($p < 0.05$) differences in the antibody titers relative to the *ospC* deletion strain ("*") and between two strains relative to each other ("+") are indicated.
(TIF)

S6 Fig. Differences in tissue colonization promoted by distinct OspC variants are not affected by an adaptive immune response. C3H/HeN-SCID mice were intradermally inoculated with $1x10^4$ WT *B. burgdorferi* strain B31-A3 carrying the empty vector ("B31-A3/Vector"), B31-A3Δ*ospC* carrying the empty vector ("Vector"), B31-A3Δ*ospC* exogenously producing OspC from *B. burgdorferi* strain B31-A3 ("B31"), N40 clone D10/E9 ("N40-D10/E9"), or *B. garinii* strain PBr ("PBr") under control of the *ospC* promoter from B31-A3. Tissues were harvested at 21 days post infection, and bacterial genomes were quantified in each tissue by qPCR. Shown are the geometric mean of bacterial loads ± 95% confidence interval of 10 mice per group. Statistical significance was determined using ANOVA with the Kruskal-Wallis test followed by the two-stage step-up method of Benjamini, Krieger and Yekutieli. Significant ($p < 0.05$) differences in spirochete number relative to the *ospC* deletion strain ("*") and between two strains relative to each other ("+") are indicated.
(TIF)

S1 Table. Bacterial strains.
(PDF)

S2 Table. Oligonucleotides.
(PDF)

S3 Table. pBSV2:chromosome ratio during in vitro culture.
(PDF)

S4 Table. OspC-encoding plasmids are retained at 21 days post-infection in Experiment 1.
(PDF)

S5 Table. OspC-encoding plasmids are retained at 21 days post-infection in Experiment 2.
(PDF)

S1 Text. Supplmentary materials and methods.
(PDF)

Acknowledgments

We thank Michael Pereira for assistance in analysis of OspC mutants, Ashley Marcinkiewicz and Thomas Hart in assisting plasmid generation and transformation, Priyanka Mukherjee for

performing the transformation to build strain GCB3226, Hiromi Sato for manuscript editing and suggestions, Patricia Rosa for providing us with *B. burgdorferi* strains B31-A3 and OspCK1 (Δ*ospC*), and plasmid pBSV2G, as well as for identifying the deletion at nucleotide position 67 in *orf2* or our pOspC plasmids. We thank Nikhat Parveen, Richard Marconi, and Jon Skare for critical discussion and communication of unpublished results. We also thank Jorge Benach for α-FlaB CB1 monoclonal antibody, James Baleja for help with circular dichroism, Allen Parmelee and Stephen Kwok in the Flow Cytometry Core in the Department of Pathology at Tufts University School of Medicine for assisting with flow cytometry, and Michael Waring of the Ragon Institute Imaging Core Facility for providing access to and assistance with SPR instrumentation. The intravital microscopy was performed in the Snyder Institutes's Live Cell Imaging Facility at the University of Calgary. We would like to thank Katarzyna Srevens and Pina Colarusso for for training and support with image acquisition and analysis and Genevieve Chaconas for technical support.

Author Contributions

Conceptualization: Yi-Pin Lin, Xi Tan, Jennifer A. Caine, Mildred Castellanos, George Chaconas, Jenifer Coburn, John M. Leong.

Formal analysis: Yi-Pin Lin, Xi Tan, Jennifer A. Caine, Mildred Castellanos, George Chaconas, Jenifer Coburn, John M. Leong.

Funding acquisition: George Chaconas, Jenifer Coburn, John M. Leong.

Investigation: Yi-Pin Lin, Xi Tan, Jennifer A. Caine, Mildred Castellanos, George Chaconas, Jenifer Coburn, John M. Leong.

Methodology: Yi-Pin Lin, Xi Tan, Jennifer A. Caine, Mildred Castellanos.

Project administration: George Chaconas, Jenifer Coburn, John M. Leong.

Resources: George Chaconas, Jenifer Coburn, John M. Leong.

Supervision: George Chaconas, Jenifer Coburn, John M. Leong.

Validation: Yi-Pin Lin, Xi Tan, Jennifer A. Caine, Mildred Castellanos, George Chaconas, Jenifer Coburn, John M. Leong.

Visualization: Yi-Pin Lin, Xi Tan, Jennifer A. Caine, George Chaconas, Jenifer Coburn, John M. Leong.

Writing – original draft: Yi-Pin Lin, Xi Tan, Jennifer A. Caine, George Chaconas, Jenifer Coburn, John M. Leong.

Writing – review & editing: Yi-Pin Lin, Xi Tan, Jennifer A. Caine, George Chaconas, Jenifer Coburn, John M. Leong.

References

1. Adeolu M, Gupta RS. A phylogenomic and molecular marker based proposal for the division of the genus Borrelia into two genera: the emended genus Borrelia containing only the members of the relapsing fever Borrelia, and the genus Borreliella gen. nov. containing the members of the Lyme disease Borrelia (Borrelia burgdorferi sensu lato complex). Antonie Van Leeuwenhoek. 2014; 105(6):1049–72. https://doi.org/10.1007/s10482-014-0164-x PMID: 24744012
2. Prevention. CfDCa. Lyme Disease- Data and Statistics 2015 [updated September 24; cited 2015 December 3]. Available from: http://www.cdc.gov/lyme/stats/: Centers for Disease Control. Available from: http://www.cdc.gov/lyme/stats.

3. Steere AC, Grodzicki RL, Kornblatt AN, Craft JE, Barbour AG, Burgdorfer W, et al. The spirochetal etiology of Lyme disease. N Engl J Med. 1983; 308(13):733–40. https://doi.org/10.1056/NEJM198303313081301 PMID: 6828118

4. Baranton G, Postic D, Saint Girons I, Boerlin P, Piffaretti JC, Assous M, et al. Delineation of *Borrelia burgdorferi* sensu stricto, *Borrelia garinii* sp. nov., and group VS461 associated with Lyme borreliosis. Int J Syst Bacteriol. 1992; 42(3):378–83. https://doi.org/10.1099/00207713-42-3-378 PMID: 1380285

5. van Dam AP, Kuiper H, Vos K, Widjojokusumo A, de Jongh BM, Spanjaard L, et al. Different genospecies of *Borrelia burgdorferi* are associated with distinct clinical manifestations of Lyme borreliosis. Clin Infect Dis. 1993; 17(4):708–17. https://doi.org/10.1093/clinids/17.4.708 PMID: 7903558

6. Strle F, Ruzic-Sabljic E, Cimperman J, Lotric-Furlan S, Maraspin V. Comparison of findings for patients with *Borrelia garinii* and *Borrelia afzelii* isolated from cerebrospinal fluid. Clin Infect Dis. 2006; 43(6):704–10. https://doi.org/10.1086/506936 PMID: 16912943

7. Wang G, van Dam AP, Schwartz I, Dankert J. Molecular typing of *Borrelia burgdorferi* sensu lato: taxonomic, epidemiological, and clinical implications. Clin Microbiol Rev. 1999; 12(4):633–53. PMID: 10515907

8. Moriarty TJ, Norman MU, Colarusso P, Bankhead T, Kubes P, Chaconas G. Real-time high resolution 3D imaging of the lyme disease spirochete adhering to and escaping from the vasculature of a living host. PLoS Pathog. 2008; 4(6):e1000090. https://doi.org/10.1371/journal.ppat.1000090 PMID: 18566656

9. Norman MU, Moriarty TJ, Dresser AR, Millen B, Kubes P, Chaconas G. Molecular mechanisms involved in vascular interactions of the Lyme disease pathogen in a living host. PLoS Pathog. 2008; 4(10):e1000169. https://doi.org/10.1371/journal.ppat.1000169 PMID: 18833295

10. Brissette CA, Gaultney RA. That's my story, and I'm sticking to it—an update on B. burgdorferi adhesins. Front Cell Infect Microbiol. 2014; 4:41. https://doi.org/10.3389/fcimb.2014.00041 PMID: 24772392

11. Hyde JA. Borrelia burgdorferi Keeps Moving and Carries on: A Review of Borrelial Dissemination and Invasion. Front Immunol. 2017; 8:114. https://doi.org/10.3389/fimmu.2017.00114 PMID: 28270812

12. Coburn J, Leong J, Chaconas G. Illuminating the roles of the *Borrelia burgdorferi* adhesins. Trends Microbiol. 2013; 21(8):372–9. https://doi.org/10.1016/j.tim.2013.06.005 PMID: 23876218

13. Weening EH, Parveen N, Trzeciakowski JP, Leong JM, Hook M, Skare JT. *Borrelia burgdorferi* lacking DbpBA exhibits an early survival defect during experimental infection. Infect Immun. 2008; 76(12):5694–705. https://doi.org/10.1128/IAI.00690-08 PMID: 18809667

14. Seshu J, Esteve-Gassent MD, Labandeira-Rey M, Kim JH, Trzeciakowski JP, Hook M, et al. Inactivation of the fibronectin-binding adhesin gene *bbk32* significantly attenuates the infectivity potential of *Borrelia burgdorferi*. Mol Microbiol. 2006; 59(5):1591–601. https://doi.org/10.1111/j.1365-2958.2005.05042.x PMID: 16468997

15. Yang X, Lenhart TR, Kariu T, Anguita J, Akins DR, Pal U. Characterization of unique regions of *Borrelia burgdorferi* surface-located membrane protein 1. Infect Immun. 2010; 78(11):4477–87. https://doi.org/10.1128/IAI.00501-10 PMID: 20696833

16. Pal U, Wang P, Bao F, Yang X, Samanta S, Schoen R, et al. *Borrelia burgdorferi* basic membrane proteins A and B participate in the genesis of Lyme arthritis. J Exp Med. 2008; 205(1):133–41. https://doi.org/10.1084/jem.20070962 PMID: 18166585

17. Brissette CA, Bykowski T, Cooley AE, Bowman A, Stevenson B. *Borrelia burgdorferi* RevA antigen binds host fibronectin. Infect Immun. 2009; 77(7):2802–12. https://doi.org/10.1128/IAI.00227-09 PMID: 19398540

18. Caine JA, Coburn J. A short-term *Borrelia burgdorferi* infection model identifies tissue tropisms and bloodstream survival conferred by adhesion proteins. Infect Immun. 2015; 83(8):3184–94. https://doi.org/10.1128/IAI.00349-15 PMID: 26015482

19. Byram R, Gaultney RA, Floden AM, Hellekson C, Stone BL, Bowman A, et al. *Borrelia burgdorferi* RevA Significantly Affects Pathogenicity and Host Response in the Mouse Model of Lyme Disease. Infect Immun. 2015; 83(9):3675–83. https://doi.org/10.1128/IAI.00530-15 PMID: 26150536

20. Lin YP, Chen Q, Ritchie JA, Dufour NP, Fischer JR, Coburn J, et al. Glycosaminoglycan binding by *Borrelia burgdorferi* adhesin BBK32 specifically and uniquely promotes joint colonization. Cell Microbiol. 2015; 17(6):860–75. https://doi.org/10.1111/cmi.12407 PMID: 25486989

21. Fortune DE, Lin YP, Deka RK, Groshong AM, Moore BP, Hagman KE, et al. Identification of Lysine Residues in the *Borrelia burgdorferi* DbpA Adhesin Required for Murine Infection. Infect Immun. 2014.

22. Lin YP, Benoit V, Yang X, Martinez-Herranz R, Pal U, Leong JM. Strain-specific variation of the decorin-binding adhesin DbpA influences the tissue tropism of the lyme disease spirochete. PLoS Pathog. 2014; 10(7):e1004238. https://doi.org/10.1371/journal.ppat.1004238 PMID: 25079227

23. Salo J, Loimaranta V, Lahdenne P, Viljanen MK, Hytonen J. Decorin binding by DbpA and B of *Borrelia garinii*, *Borrelia afzelii*, and *Borrelia burgdorferi* sensu Stricto. J Infect Dis. 2011; 204(1):65–73. https://doi.org/10.1093/infdis/jir207 PMID: 21628660

24. Benoit VM, Fischer JR, Lin YP, Parveen N, Leong JM. Allelic variation of the Lyme disease spirochete adhesin DbpA influences spirochetal binding to decorin, dermatan sulfate, and mammalian cells. Infect Immun. 2011; 79(9):3501–9. https://doi.org/10.1128/IAI.00163-11 PMID: 21708995

25. Schwan TG, Piesman J, Golde WT, Dolan MC, Rosa PA. Induction of an outer surface protein on *Borrelia burgdorferi* during tick feeding. Proc Natl Acad Sci U S A. 1995; 92(7):2909–13. https://doi.org/10.1073/pnas.92.7.2909 PMID: 7708747

26. Grimm D, Tilly K, Byram R, Stewart PE, Krum JG, Bueschel DM, et al. Outer-surface protein C of the Lyme disease spirochete: a protein induced in ticks for infection of mammals. Proc Natl Acad Sci U S A. 2004; 101(9):3142–7. https://doi.org/10.1073/pnas.0306845101 PMID: 14970347

27. Pal U, Yang X, Chen M, Bockenstedt LK, Anderson JF, Flavell RA, et al. OspC facilitates *Borrelia burgdorferi* invasion of *Ixodes scapularis* salivary glands. J Clin Invest. 2004; 113(2):220–30. https://doi.org/10.1172/JCI19894 PMID: 14722614

28. Tilly K, Krum JG, Bestor A, Jewett MW, Grimm D, Bueschel D, et al. *Borrelia burgdorferi* OspC protein required exclusively in a crucial early stage of mammalian infection. Infect Immun. 2006; 74(6):3554–64. https://doi.org/10.1128/IAI.01950-05 PMID: 16714588

29. Brisson D, Drecktrah D, Eggers CH, Samuels DS. Genetics of *Borrelia burgdorferi*. Annu Rev Genet. 2012; 46:515–36. https://doi.org/10.1146/annurev-genet-011112-112140 PMID: 22974303

30. Chaconas G, Castellanos M, Verhey TB. Changing of the guard: How the Lyme disease spirochete subverts the host immune response. J Biol Chem. 2019; 295: 301–13. https://doi.org/10.1074/jbc.REV119.008583 PMID: 31753921

31. Norris SJ. vls Antigenic Variation Systems of Lyme Disease Borrelia: Eluding Host Immunity through both Random, Segmental Gene Conversion and Framework Heterogeneity. Microbiol Spectr. 2014; 2 (6).

32. Wilske B, Preac-Mursic V, Jauris S, Hofmann A, Pradel I, Soutschek E, et al. Immunological and molecular polymorphisms of OspC, an immunodominant major outer surface protein of *Borrelia burgdorferi*. Infect Immun. 1993; 61(5):2182–91. PMID: 8478108

33. Lin T, Oliver JH Jr., Gao L. Genetic diversity of the outer surface protein C gene of southern *Borrelia* isolates and its possible epidemiological, clinical, and pathogenetic implications. J Clin Microbiol. 2002; 40 (7):2572–83. https://doi.org/10.1128/JCM.40.7.2572-2583.2002 PMID: 12089279

34. Seinost G, Dykhuizen DE, Dattwyler RJ, Golde WT, Dunn JJ, Wang IN, et al. Four clones of *Borrelia burgdorferi* sensu stricto cause invasive infection in humans. Infect Immun. 1999; 67(7):3518–24. PMID: 10377134

35. Earnhart CG, Buckles EL, Dumler JS, Marconi RT. Demonstration of OspC type diversity in invasive human lyme disease isolates and identification of previously uncharacterized epitopes that define the specificity of the OspC murine antibody response. Infect Immun. 2005; 73(12):7869–77. https://doi.org/10.1128/IAI.73.12.7869-7877.2005 PMID: 16299277

36. Wang IN, Dykhuizen DE, Qiu W, Dunn JJ, Bosler EM, Luft BJ. Genetic diversity of ospC in a local population of *Borrelia burgdorferi* sensu stricto. Genetics. 1999; 151(1):15–30. PMID: 9872945

37. Lagal V, Postic D, Ruzic-Sabljic E, Baranton G. Genetic diversity among *Borrelia* strains determined by single-strand conformation polymorphism analysis of the *ospC* gene and its association with invasiveness. J Clin Microbiol. 2003; 41(11):5059–65. https://doi.org/10.1128/JCM.41.11.5059-5065.2003 PMID: 14605139

38. Wang G, Ojaimi C, Iyer R, Saksenberg V, McClain SA, Wormser GP, et al. Impact of genotypic variation of *Borrelia burgdorferi* sensu stricto on kinetics of dissemination and severity of disease in C3H/HeJ mice. Infect Immun. 2001; 69(7):4303–12. https://doi.org/10.1128/IAI.69.7.4303-4312.2001 PMID: 11401967

39. Iyer R, Liveris D, Adams A, Nowakowski J, McKenna D, Bittker S, et al. Characterization of *Borrelia burgdorferi* isolated from erythema migrans lesions: interrelationship of three molecular typing methods. J Clin Microbiol. 2001; 39(8):2954–7. https://doi.org/10.1128/JCM.39.8.2954-2957.2001 PMID: 11474020

40. Wang G, Ojaimi C, Wu H, Saksenberg V, Iyer R, Liveris D, et al. Disease severity in a murine model of lyme borreliosis is associated with the genotype of the infecting *Borrelia burgdorferi* sensu stricto strain. J Infect Dis. 2002; 186(6):782–91. https://doi.org/10.1086/343043 PMID: 12198612

41. Onder O, Humphrey PT, McOmber B, Korobova F, Francella N, Greenbaum DC, et al. OspC is potent plasminogen receptor on surface of *Borrelia burgdorferi*. J Biol Chem. 2012; 287(20):16860–8. https://doi.org/10.1074/jbc.M111.290775 PMID: 22433849

42. Carrasco SE, Troxell B, Yang Y, Brandt SL, Li H, Sandusky GE, et al. Outer surface protein OspC is an antiphagocytic factor that protects *Borrelia burgdorferi* from phagocytosis by macrophages. Infect Immun. 2015; 83(12):4848–60. https://doi.org/10.1128/IAI.01215-15 PMID: 26438793

43. Caine JA, Lin YP, Kessler JR, Sato H, Leong JM, Coburn J. Borrelia burgdorferi outer surface protein C (OspC) binds complement component C4b and confers bloodstream survival. Cell Microbiol. 2017. https://doi.org/10.1111/cmi.12786 PMID: 28873507

44. Cadavid D, Pennington PM, Kerentseva TA, Bergstrom S, Barbour AG. Immunologic and genetic analyses of VmpA of a neurotropic strain of *Borrelia turicatae*. Infect Immun. 1997; 65(8):3352–60. PMID: 9234797

45. Zuckert WR, Kerentseva TA, Lawson CL, Barbour AG. Structural conservation of neurotropism-associated VspA within the variable *Borrelia* Vsp-OspC lipoprotein family. J Biol Chem. 2001; 276(1):457–63. https://doi.org/10.1074/jbc.M008449200 PMID: 11018048

46. Schwan TG, Raffel SJ, Battisti JM. Transgenic functional complementation with a transmission -associated protein restores spirochete infectivity by tick bite. Ticks Tick Borne Dis. 2020; 11:101377. https://doi.org/10.1016/j.ttbdis.2020.101377 PMID: 32005628

47. Magoun L, Zuckert WR, Robbins D, Parveen N, Alugupalli KR, Schwan TG, et al. Variable small protein (Vsp)-dependent and Vsp-independent pathways for glycosaminoglycan recognition by relapsing fever spirochaetes. Mol Microbiol. 2000; 36(4):886–97. https://doi.org/10.1046/j.1365-2958.2000.01906.x PMID: 10844676

48. Pennington PM, Allred CD, West CS, Alvarez R, Barbour AG. Arthritis severity and spirochete burden are determined by serotype in the *Borrelia turicatae*-mouse model of Lyme disease. Infect Immun. 1997; 65(1):285–92. PMID: 8975925

49. Antonara S, Chafel RM, LaFrance M, Coburn J. *Borrelia burgdorferi* adhesins identified using *in vivo* phage display. Mol Microbiol. 2007; 66(1):262–76. https://doi.org/10.1111/j.1365-2958.2007.05924.x PMID: 17784908

50. Moriarty TJ, Shi M, Lin YP, Ebady R, Zhou H, Odisho T, et al. Vascular binding of a pathogen under shear force through mechanistically distinct sequential interactions with host macromolecules. Mol Microbiol. 2012; 86(5):1116–31. https://doi.org/10.1111/mmi.12045 PMID: 23095033

51. Gaultney RA, Gonzalez T, Floden AM, Brissette CA. BB0347, from the lyme disease spirochete Borrelia burgdorferi, is surface exposed and interacts with the CS1 heparin-binding domain of human fibronectin. PLoS One. 2013; 8(9):e75643. https://doi.org/10.1371/journal.pone.0075643 PMID: 24086600

52. Probert WS, Johnson BJ. Identification of a 47 kDa fibronectin-binding protein expressed by *Borrelia burgdorferi* isolate B31. Mol Microbiol. 1998; 30(5):1003–15. https://doi.org/10.1046/j.1365-2958.1998.01127.x PMID: 9988477

53. Probert WS, Kim JH, Hook M, Johnson BJ. Mapping the ligand-binding region of *Borrelia burgdorferi* fibronectin-binding protein BBK32. Infect Immun. 2001; 69(6):4129–33. https://doi.org/10.1128/IAI.69.6.4129-4133.2001 PMID: 11349087

54. Fischer JR, LeBlanc KT, Leong JM. Fibronectin binding protein BBK32 of the Lyme disease spirochete promotes bacterial attachment to glycosaminoglycans. Infect Immun. 2006; 74(1):435–41. https://doi.org/10.1128/IAI.74.1.435-441.2006 PMID: 16368999

55. Parveen N, Caimano M, Radolf JD, Leong JM. Adaptation of the Lyme disease spirochaete to the mammalian host environment results in enhanced glycosaminoglycan and host cell binding. Mol Microbiol. 2003; 47(5):1433–44. https://doi.org/10.1046/j.1365-2958.2003.03388.x PMID: 12603746

56. Lin YP, Bhowmick R, Coburn J, Leong JM. Host cell heparan sulfate glycosaminoglycans are ligands for OspF-related proteins of the Lyme disease spirochete. Cell Microbiol. 2015; 17(10):1464–76. https://doi.org/10.1111/cmi.12448 PMID: 25864455

57. Yang X, Lin YP, Heselpoth RD, Buyuktanir O, Qin J, Kung F, et al. Middle region of the Borrelia burgdorferi surface-located protein 1 (Lmp1) interacts with host chondroitin-6-sulfate and independently facilitates infection. Cell Microbiol. 2016; 18(1):97–110. https://doi.org/10.1111/cmi.12487 PMID: 26247174

58. Hileman RE, Fromm JR, Weiler JM, Linhardt RJ. Glycosaminoglycan-protein interactions: definition of consensus sites in glycosaminoglycan binding proteins. Bioessays. 1998; 20(2):156–67. https://doi.org/10.1002/(SICI)1521-1878(199802)20:2<156::AID-BIES8>3.0.CO;2-R PMID: 9631661

59. Parveen N, Leong JM. Identification of a candidate glycosaminoglycan-binding adhesin of the Lyme disease spirochete *Borrelia burgdorferi*. Mol Microbiol. 2000; 35(5):1220–34. https://doi.org/10.1046/j.1365-2958.2000.01792.x PMID: 10712702

60. Guo BP, Brown EL, Dorward DW, Rosenberg LC, Hook M. Decorin-binding adhesins from *Borrelia burgdorferi*. Mol Microbiol. 1998; 30(4):711–23. https://doi.org/10.1046/j.1365-2958.1998.01103.x PMID: 10094620

61. Fischer JR, Parveen N, Magoun L, Leong JM. Decorin-binding proteins A and B confer distinct mammalian cell type-specific attachment by *Borrelia burgdorferi*, the Lyme disease spirochete. Proc Natl Acad Sci U S A. 2003; 100(12):7307–12. https://doi.org/10.1073/pnas.1231043100 PMID: 12773620

62. Kumar D, Ristow LC, Shi M, Mukherjee P, Caine JA, Lee WY, et al. Intravital Imaging of Vascular Transmigration by the Lyme Spirochete: Requirement for the Integrin Binding Residues of the B. burgdorferi P66 Protein. PLoS Pathog. 2015; 11(12):e1005333. https://doi.org/10.1371/journal.ppat.1005333 PMID: 26684456

63. Lee WY, Moriarty TJ, Wong CH, Zhou H, Strieter RM, van Rooijen N, et al. An intravascular immune response to *Borrelia burgdorferi* involves Kupffer cells and iNKT cells. Nat Immunol. 2010; 11(4):295–302. https://doi.org/10.1038/ni.1855 PMID: 20228796

64. Lee WY, Sanz MJ, Wong CH, Hardy PO, Salman-Dilgimen A, Moriarty TJ, et al. Invariant natural killer T cells act as an extravascular cytotoxic barrier for joint-invading Lyme Borrelia. Proc Natl Acad Sci U S A. 2014; 111(38):13936–41. https://doi.org/10.1073/pnas.1404769111 PMID: 25205813

65. Xu Q, Seemanapalli SV, McShan K, Liang FT. Constitutive expression of outer surface protein C diminishes the ability of *Borrelia burgdorferi* to evade specific humoral immunity. Infect Immun. 2006; 74 (9):5177–84. https://doi.org/10.1128/IAI.00713-06 PMID: 16926410

66. Stewart PE, Wang X, Bueschel DM, Clifton DR, Grimm D, Tilly K, et al. Delineating the requirement for the *Borrelia burgdorferi* virulence factor OspC in the mammalian host. Infect Immun. 2006; 74(6):3547–53. https://doi.org/10.1128/IAI.00158-06 PMID: 16714587

67. Dykhuizen DE, Brisson D, Sandigursky S, Wormser GP, Nowakowski J, Nadelman RB, et al. The propensity of different *Borrelia burgdorferi* sensu stricto genotypes to cause disseminated infections in humans. Am J Trop Med Hyg. 2008; 78(5):806–10. PMID: 18458317

68. Wormser GP, Brisson D, Liveris D, Hanincova K, Sandigursky S, Nowakowski J, et al. *Borrelia burgdorferi* genotype predicts the capacity for hematogenous dissemination during early Lyme disease. J Infect Dis. 2008; 198(9):1358–64. https://doi.org/10.1086/592279 PMID: 18781866

69. Lagal V, Portnoi D, Faure G, Postic D, Baranton G. *Borrelia burgdorferi* sensu stricto invasiveness is correlated with OspC-plasminogen affinity. Microbes Infect. 2006; 8(3):645–52. https://doi.org/10.1016/j.micinf.2005.08.017 PMID: 16513394

70. Schlachter S, Seshu J, Lin T, Norris S, Parveen N. The *Borrelia burgdorferi* Glycosaminoglycan Binding Protein Bgp in the B31 Strain Is Not Essential for Infectivity despite Facilitating Adherence and Tissue Colonization. Infect Immun. 2018; 86(2). https://doi.org/10.1128/IAI.00667-17 PMID: 29158428

71. Voss B, Glossl J, Cully Z, Kresse H. Immunocytochemical investigation on the distribution of small chondroitin sulfate-dermatan sulfate proteoglycan in the human. J Histochem Cytochem. 1986; 34 (8):1013–9. https://doi.org/10.1177/34.8.2426331 PMID: 2426331

72. Sabbagh MF, Heng JS, Luo C, Castanon RG, Nery JR, Rattner A, et al. Transcriptional and epigenomic landscapes of CNS and non-CNS vascular endothelial cells. Elife. 2018; 7. https://doi.org/10.7554/eLife.36187 PMID: 30188322

73. Arap W, Kolonin MG, Trepel M, Lahdenranta J, Cardo-Vila M, Giordano RJ, et al. Steps toward mapping the human vasculature by phage display. Nat Med. 2002; 8(2):121–7. https://doi.org/10.1038/nm0202-121 PMID: 11821895

74. Pasqualini R, Ruoslahti E. Organ targeting in vivo using phage display peptide libraries. Nature. 1996; 380(6572):364–6. https://doi.org/10.1038/380364a0 PMID: 8598934

75. Rajotte D, Arap W, Hagedorn M, Koivunen E, Pasqualini R, Ruoslahti E. Molecular heterogeneity of the vascular endothelium revealed by *in vivo* phage display. J Clin Invest. 1998; 102(2):430–7. https://doi.org/10.1172/JCI3008 PMID: 9664085

76. Ebady R, Niddam AF, Boczula AE, Kim YR, Gupta N, Tang TT, et al. Biomechanics of *Borrelia burgdorferi* Vascular Interactions. Cell Rep. 2016; 16(10):2593–604. https://doi.org/10.1016/j.celrep.2016.08.013 PMID: 27568563

77. Niddam AF, Ebady R, Bansal A, Koehler A, Hinz B, Moriarty TJ. Plasma fibronectin stabilizes *Borrelia burgdorferi*-endothelial interactions under vascular shear stress by a catch-bond mechanism. Proc Natl Acad Sci U S A. 2017; 114(17):E3490–E8. https://doi.org/10.1073/pnas.1615007114 PMID: 28396443

78. Sackstein R. The lymphocyte homing receptors: gatekeepers of the multistep paradigm. Curr Opin Hematol. 2005; 12(6):444–50. https://doi.org/10.1097/01.moh.0000177827.78280.79 PMID: 16217160

79. Parish CR. The role of heparan sulphate in inflammation. Nat Rev Immunol. 2006; 6(9):633–43. https://doi.org/10.1038/nri1918 PMID: 16917509

80. Barbour AG. Isolation and cultivation of Lyme disease spirochetes. Yale J Biol Med. 1984; 57(4):521–5. PMID: 6393604

81. Bunikis I, Kutschan-Bunikis S, Bonde M, Bergstrom S. Multiplex PCR as a tool for validating plasmid content of *Borrelia burgdorferi*. J Microbiol Methods. 2011; 86(2):243–7. https://doi.org/10.1016/j.mimet.2011.05.004 PMID: 21605603

82. Elias AF, Stewart PE, Grimm D, Caimano MJ, Eggers CH, Tilly K, et al. Clonal polymorphism of *Borrelia burgdorferi* strain B31 MI: implications for mutagenesis in an infectious strain background. Infect Immun. 2002; 70(4):2139–50. https://doi.org/10.1128/IAI.70.4.2139-2150.2002 PMID: 11895980

83. Purser JE, Norris SJ. Correlation between plasmid content and infectivity in *Borrelia burgdorferi*. Proc Natl Acad Sci U S A. 2000; 97(25):13865–70. https://doi.org/10.1073/pnas.97.25.13865 PMID: 11106398

84. Chiu J, March PE, Lee R, Tillett D. Site-directed, Ligase-Independent Mutagenesis (SLIM): a single-tube methodology approaching 100% efficiency in 4 h. Nucleic Acids Res. 2004; 32(21):e174. https://doi.org/10.1093/nar/gnh172 PMID: 15585660

85. Purser JE, Lawrenz MB, Caimano MJ, Howell JK, Radolf JD, Norris SJ. A plasmid-encoded nicotinamidase (PncA) is essential for infectivity of Borrelia burgdorferi in a mammalian host. Mol Microbiol. 2003; 48(3):753–64. https://doi.org/10.1046/j.1365-2958.2003.03452.x PMID: 12694619

86. Dresser AR, Hardy PO, Chaconas G. Investigation of the genes involved in antigenic switching at the vlsE locus in Borrelia burgdorferi: an essential role for the RuvAB branch migrase. PLoS Pathog. 2009; 5(12):e1000680. https://doi.org/10.1371/journal.ppat.1000680 PMID: 19997508

87. Lin YP, Lee DW, McDonough SP, Nicholson LK, Sharma Y, Chang YF. Repeated domains of leptospira immunoglobulin-like proteins interact with elastin and tropoelastin. J Biol Chem. 2009; 284(29):19380–91. https://doi.org/10.1074/jbc.M109.004531 PMID: 19473986

88. Liveris D, Wang G, Girao G, Byrne DW, Nowakowski J, McKenna D, et al. Quantitative detection of *Borrelia burgdorferi* in 2-millimeter skin samples of erythema migrans lesions: correlation of results with clinical and laboratory findings. J Clin Microbiol. 2002; 40(4):1249–53. https://doi.org/10.1128/JCM.40.4.1249-1253.2002 PMID: 11923340

89. Yang X, Coleman AS, Anguita J, Pal U. A chromosomally encoded virulence factor protects the Lyme disease pathogen against host-adaptive immunity. PLoS Pathog. 2009; 5(3):e1000326. https://doi.org/10.1371/journal.ppat.1000326 PMID: 19266024

90. Hall TA. BioEdit: a user-friendly biological sequence alignment editor and analysis program for Windows 95/98/NT. Nucl Acds Symp Ser 1999; 41:95–8.

91. Eicken C, Sharma V, Klabunde T, Owens RT, Pikas DS, Hook M, et al. Crystal structure of Lyme disease antigen outer surface protein C from *Borrelia burgdorferi*. J Biol Chem. 2001; 276(13):10010–5. https://doi.org/10.1074/jbc.M010062200 PMID: 11139584

92. Kumaran D, Eswaramoorthy S, Luft BJ, Koide S, Dunn JJ, Lawson CL, et al. Crystal structure of outer surface protein C (OspC) from the Lyme disease spirochete, Borrelia burgdorferi. EMBO J. 2001; 20(5):971–8. https://doi.org/10.1093/emboj/20.5.971 PMID: 11230121